Multi-Source Hydrological Data Products to Monitor High Asian River Basins and Regional Water Security

Menenti, Massimo; Li, Xin; Jia, Li; Yang, Kun; Pellicciotti, Francesca; Mancini, Marco; Shi, Jiancheng; Escorihuela, Maria José; Zheng, Chaolei; More Authors

DOI
10.3390/rs13245122

Publication date
2021

Document Version
Final published version

Published in
Remote Sensing

Citation (APA)
Menenti, M., Li, X., Jia, L., Yang, K., Pellicciotti, F., Mancini, M., Shi, J., Escorihuela, M. J., Zheng, C., & More Authors (2021). Multi-Source Hydrological Data Products to Monitor High Asian River Basins and Regional Water Security. *Remote Sensing*, *13*(24), Article 5122. https://doi.org/10.3390/rs13245122

remote sensing

MDPI

Project Report

Multi-Source Hydrological Data Products to Monitor High Asian River Basins and Regional Water Security

Massimo Menenti [1,2,*], Xin Li [3], Li Jia [2], Kun Yang [4], Francesca Pellicciotti [5], Marco Mancini [6], Jiancheng Shi [7], Maria José Escorihuela [8], Chaolei Zheng [2], Qiting Chen [2], Jing Lu [2], Jie Zhou [2], Guangcheng Hu [2], Shaoting Ren [2], Jing Zhang [2], Qinhuo Liu [2], Yubao Qiu [2], Chunlin Huang [9], Ji Zhou [10], Xujun Han [9], Xiaoduo Pan [3], Hongyi Li [9], Yerong Wu [11], Baohong Ding [3], Wei Yang [3], Pascal Buri [5], Michael J. McCarthy [5], Evan S. Miles [5], Thomas E. Shaw [5], Chunfeng Ma [9], Yanzhao Zhou [2], Chiara Corbari [6], Rui Li [2], Tianjie Zhao [2], Vivien Stefan [8], Qi Gao [8], Jingxiao Zhang [2], Qiuxia Xie [2], Ning Wang [2], Yibo Sun [2], Xinyu Mo [2], Junru Jia [2], Achille Pierre Jouberton [5], Marin Kneib [5], Stefan Fugger [5], Nicola Paciolla [6] and Giovanni Paolini [8]

[1] Faculty of Civil Engineering and Earth Sciences, Delft University of Technology, 2628 Delft, The Netherlands
[2] State Key Laboratory of Remote Sensing Science, Aerospace Information Research Institute, Chinese Academy of Sciences, Beijing 100101, China; jiali@aircas.ac.cn (L.J.); zhengcl@radi.ac.cn (C.Z.); chenqt@radi.ac.cn (Q.C.); lujing@radi.ac.cn (J.L.); zhou.j@mail.ccnu.edu.cn (J.Z.); hugc@radi.ac.cn (G.H.); renst@radi.ac.cn (S.R.); zhangjing2015@radi.ac.cn (J.Z.); liuqh@radi.ac.cn (Q.L.); qiuyb@aircas.ac.cn (Y.Q.); lirui@radi.ac.cn (R.L.); zhaoyanzhao@lzb.ac.cn (Y.Z.); zhaotj@aircas.ac.cn (T.Z.); zhangjx@radi.ac.cn (J.Z.); xieqx@radi.ac.cn (Q.X.); remote_gis@163.com (N.W.); sunyb@radi.ac.cn (Y.S.); moxy@radi.ac.cn (X.M.); jiajr@radi.ac.cn (J.J.)
[3] Institute of Tibetan Plateau Research, Chinese Academy of Sciences, Beijing 100101, China; lixin@itpcas.ac.cn (X.L.); panxd@itpcas.ac.cn (X.P.); dingbh@itpcas.ac.cn (B.D.); yangww@itpcas.ac.cn (W.Y.)
[4] Department of Earth System Science, Tsinghua University, Beijing 100084, China; yangk@tsinghua.edu.cn
[5] Swiss Federal Institute for Forest, Snow and Landscape Research WSL, 8903 Birmensdorf, Switzerland; francesca.pellicciotti@wsl.ch (F.P.); pascal.buri@wsl.ch (P.B.); michael.mccarthy@wsl.ch (M.J.M.); evan.miles@wsl.ch (E.S.M.); thomas.shaw@wsl.ch (T.E.S.); achille.jouberton@wsl.ch (A.P.J.); marin.kneib@wsl.ch (M.K.); stefan.fugger@wsl.ch (S.F.)
[6] Department of Civil and Environmental Engineering (DICA), Politecnico di Milano, 20133 Milano, Italy; marco.mancini@polimi.it (M.M.); chiara.corbari@polimi.it (C.C.); nicola.paciolla@polimi.it (N.P.); giovanni.paolini@isardsat.cat (G.P.)
[7] The National Space Science Center, Chinese Academy of Sciences, Beijing 100190, China; shijiancheng@nssc.ac.cn
[8] isardSAT, Parc Tecnològic Barcelona Activa, Carrer de Marie Curie, 8, 08042 Barcelona, Spain; mj.escorihuela@isardsat.cat (M.J.E.); vivien.stefan@isardsat.cat (V.S.); qi.gao@isardsat.cat (Q.G.)
[9] Northwest Institute of Eco-Environment and Resources, Chinese Academy of Sciences, Lanzhou 730000, China; huangcl@lzb.ac.cn (C.H.); hanxj@lzb.ac.cn (X.H.); lihongyi@lzb.ac.cn (H.L.); machf@lzb.ac.cn (C.M.)
[10] School of Resources and Environment, Center for Information Geoscience, University of Electronic Science and Technology of China, Chengdu 610054, China; jzhou233@uestc.edu.cn
[11] National-Local Jonit Engineering Laboratory of Geo-Spatial Information Technology, Hunan University of Science and Technology, Xiangtan 411201, China; yerong.wu@hnust.edu.cn
* Correspondence: M.Menenti@tudelft.nl; Tel.: +31-6-3943-0621

check for updates

Citation: Menenti, M.; Li, X.; Jia, L.; Yang, K.; Pellicciotti, F.; Mancini, M.; Shi, J.; Escorihuela, M.J.; Zheng, C.; Chen, Q.; et al. Multi-Source Hydrological Data Products to Monitor High Asian River Basins and Regional Water Security. *Remote Sens.* **2021**, *13*, 5122. https://doi.org/10.3390/rs13245122

Academic Editor: Sayed M. Bateni

Received: 13 October 2021
Accepted: 6 December 2021
Published: 16 December 2021

Abstract: This project explored the integrated use of satellite, ground observations and hydrological distributed models to support water resources assessment and monitoring in High Mountain Asia (HMA). Hydrological data products were generated taking advantage of the synergies of European and Chinese data assets and space-borne observation systems. Energy-budget-based glacier mass balance and hydrological models driven by satellite observations were developed. These models can be applied to describe glacier-melt contribution to river flow. Satellite hydrological data products were used for forcing, calibration, validation and data assimilation in distributed river basin models. A pilot study was carried out on the Red River basin. Multiple hydrological data products were generated using the data collected by Chinese satellites. A new Evapo-Transpiration (ET) dataset from 2000 to 2018 was generated, including plant transpiration, soil evaporation, rainfall interception loss, snow/ice sublimation and open water evaporation. Higher resolution data were used to characterize glaciers and their response to environmental forcing. These studies focused on the Parlung Zangbo Basin, where glacier facies were mapped with GaoFeng (GF), Sentinal-2/Multi-Spectral Imager (S2/MSI) and Landsat8/Operational Land Imager (L8/OLI) data. The geodetic mass

balance was estimated between 2000 and 2017 with Zi-Yuan (ZY)-3 Stereo Images and the SRTM DEM. Surface velocity was studied with Landsat5/Thematic Mapper (L5/TM), L8/OLI and S2/MSI data over the period 2013–2019. An updated method was developed to improve the retrieval of glacier albedo by correcting glacier reflectance for anisotropy, and a new dataset on glacier albedo was generated for the period 2001–2020. A detailed glacier energy and mass balance model was developed with the support of field experiments at the Parlung No. 4 Glacier and the 24 K Glacier, both in the Tibetan Plateau. Besides meteorological measurements, the field experiments included glaciological and hydrological measurements. The energy balance model was formulated in terms of enthalpy for easier treatment of water phase transitions. The model was applied to assess the spatial variability in glacier melt. In the Parlung No. 4 Glacier, the accumulated glacier melt was between 1.5 and 2.5 m w.e. in the accumulation zone and between 4.5 and 6.0 m w.e. in the ablation zone, reaching 6.5 m w.e. at the terminus. The seasonality in the glacier mass balance was observed by combining intensive field campaigns with continuous automatic observations. The linkage of the glacier and snowpack mass balance with water resources in a river basin was analyzed in the Chiese (Italy) and Heihe (China) basins by developing and applying integrated hydrological models using satellite retrievals in multiple ways. The model FEST-WEB was calibrated using retrievals of Land Surface Temperature (LST) to map soil hydrological properties. A watershed model was developed by coupling ecohydrological and socioeconomic systems. Integrated modeling is supported by an updated and parallelized data assimilation system. The latter exploits retrievals of brightness temperature (Advanced Microwave Scanning Radiometer, AMSR), LST (Moderate Resolution Imaging Spectroradiometer, MODIS), precipitation (Tropical Rainfall Measuring Mission (TRMM) and FengYun (FY)-2D) and in-situ measurements. In the case study on the Red River Basin, a new algorithm has been applied to disaggregate the SMOS (Soil Moisture and Ocean Salinity) soil moisture retrievals by making use of the correlation between evaporative fraction and soil moisture.

Keywords: High Mountain Asia; multispectral remote sensing; distributed hydrological models; energy and water balance; model calibration; data assimilation

1. Introduction

This report describes one of the projects (see title of the study) carried out under the Dragon 4 program in the period 2016–2020. The goal of the project was two-fold: (a) observation and modeling of the terrestrial water cycle at high elevation; (b) develop and evaluate methods to use efficiently the growing suite of satellite data products on the terrestrial water cycle.

At high elevation in general and in High Mountain Asia in particular, the expected increase in air temperatures will have far-reaching and complex impacts on the terrestrial water cycle and is likely to increase the fraction of liquid precipitation. Snow cover will be seasonal up to higher elevation. These changes will deeply modify water supply to lower elevation areas in South and East (S and E) Asia [1].

This project builds upon a previous effort (see [2]) to build and apply a regional hydrological model to describe cryospheric and hydrospheric processes in the entire region, including the Tibetan Plateau and the surrounding river basins.

Human life and the entire ecosystem of S and E Asia depend upon the monsoon climate and its predictability. More than 40% of the earth's population lives in this region. Droughts and floods associated with the variability of rainfall frequently cause serious damage to ecosystems in these regions and, more importantly, injury and loss of human life. The headwater areas of seven major rivers in S and E Asia, i.e., Yellow River, Yangtze, Mekong, Salween, Irrawaddy, Brahmaputra and Ganges, are located in the Tibetan Plateau. Estimates of the Plateau water balance rely on sparse and scarce observations that cannot provide the required accuracy, spatial density and temporal frequency.

Water Resources. The Qinghai–Tibetan Plateau, with its high altitude, unique geographical features and rich wildlife, and water and mineral resources is a unique region on Earth. The high mountain ranges, and especially the Tibetan Plateau, play a major role in the climatic system of Asia and the monsoon systems. This in turn affects global climate and global climatic change. The Tibetan Plateau has an important influence on the regional and atmospheric circulation and splits the upper westerly winds in winter into northern and southern branches [3].

Current knowledge and uncertainty on the Qinghai–Tibetan Plateau water balance. Menenti et al. [2] estimated the net hydrological flows in Tibet as 565 km^3 per year. This amounts to roughly 6% of Asia's annual runoff and 31% of India's total river water resources. Historically, negligible utilization rates in Tibet meant that nearly all of this water was transferred to countries in downstream basins including India, Nepal, China, Bangladesh, Pakistan, Bhutan, Vietnam, Burma (Myanmar), Cambodia, Laos and Thailand. Today, hydrological transfers from Tibet to other countries total 577 (546 according to other sources) $km^3\ yr^{-1}$ from a gross basin area of 1.1 million km^2. ET may increase in response to direct atmospheric forcing, in terms of solar irradiance and air temperature, rather than decrease in response to a decrease in precipitation, as shown to be the case in the Alps by [4]. The increase in ET further reduces runoff in addition to the effect of reduced precipitation.

Modeling the terrestrial water cycle in complex and heterogeneous catchments at high elevation requires high spatial (100 m) and temporal (1 day) resolution (see e.g., Wood et al. [5]), particularly to account for the effects of complex terrain and fragmented vegetation cover.

At high elevation on the Tibetan Plateau and more in general on the plateaus of Central Asia, the rapidly varying snow-cover and the large number of glaciers and glacial lakes is a particularly relevant component of heterogeneity, while it determines the contribution of High Mountain Asia (HMA) to water security in the region. These processes and interactions have been studied in-depth in Europe in an effort to understand ongoing changes and project the future role of cryospheric and hydrologic processes in ecosystem services and water security in the context of climate change (see e.g., [1]). In HMA, large research initiatives are increasingly targeting these challenges. Accurate observations to monitor the surface albedo are of particular relevance since albedo links the mass with the energy balance of the terrestrial cryosphere and land surface with boundary layer processes.

The last decade has seen an increasing interest for cryospheric and hydrologic processes in cold, high elevation regions. This is due to a two-fold relevance:

(a) The cryosphere in high elevation regions is a sensitive indicator of climate change;
(b) Meltwater from glaciers, permafrost and snow is a significant fraction, and a critical one at times, of freshwater resources in many parts of the world, particularly in China and in the countries receiving waters from the Qinghai–Tibet Plateau (Figure 1).

An analysis of recent literature shows that cryosphere and hydrology questions should be linked toward better science on the terrestrial water cycle across a range of spatial and temporal scales. This leads to the need of connecting regional and global analyses of water resources. Fully integrated use of satellite, ground observations and hydrological distributed models is necessary to support water resources management in S and E Asia and to clarify the roles of the interactions between the land surface and the atmosphere in the Tibetan Plateau in the Asian monsoon system (Figure 1).

The initial objectives of the project were:

- To generate hydrological data products taking advantage of the synergies of European and Chinese data assets and space-borne observation systems, taking advantage of the improved accessibility and standardization of Chinese data products;
- To develop an energy-budget-based glacier mass balance model driven by satellite observations and linked with a distributed river basin model to describe glacier-melt contribution to river flow;
- To use satellite hydrological data products for forcing, calibration, validation and data assimilation in basin scale hydrological models;

➢ To develop synergies between Synthetic Aperture Radar (SAR) polarimetry and SAR altimetry to map flooded areas and to delineate water bodies extent as well as to estimate their water level.

Figure 1. The Qinghai–Tibet Plateau and the watersheds receiving melt-waters from the Plateau.

The project is structured in four subprojects, each addressing one of these four objectives. This report presents first the four subprojects carried out as parts of the investigation, then describes separately the aims of each subproject and the approach applied (Section 3). Next, the results and conclusions of each subproject are detailed (Section 4). Finally, the main conclusions are summarized in Section 5.

2. Project, Sub-Projects, EO and Other Data Utilization

2.1. List of Sub-Projects and Teaming

The project was structured in four sub-projects and carried out by a large Team (Table 1).

Table 1. List of sub-projects, lead and principal investigators, and team members.

Multi-Source Hydrological Data Products to Monitor High Asian River Basins and Regional Water Security				
LI (China)	**LI Xin**	**LI (ESA)**	**Massimo MENENTI**	
Sub-Project	**PI**	**Senior Scientists**	**Junior Scientists**	**PhD Students**
Data products terrestrial water cycle	JIA Li Massimo MENENTI	LIU Qinhuo QIU Yubao	ZHENG Chaolei, CHEN Qiting, LU Jing, ZHOU Jie, HU Guangcheng, WU Yerong	ZHANG Jingxiao, REN Shaoting, XIE Qiuxia, WANG Ning, SUN Yibo, MO Xinyu, ZHANG Jing, JIA Junru
High elevation hydrological processes	YANG Kun Francesca PELLIC-CIOTTI		Baohong Ding, Wei Yang Pascal Buri, Mike McCarthy, Evan Miles, Thomas Shaw	Achille Pierre Jouberton, Marin Kneib, Stefan Fugger
Basin scale hydrological models	LI Xin Marco MANCINI	HUANG Chunlin, ZHOU Ji, HAN Xujun, PAN Xiaoduo, LI Hongyi	MA Chunfeng, ZHOU Yanzhao Chiara Corbari	Nicola Paciolla
Water resources Red River Basin	SHI Jiancheng Maria José ESCORIHUELA		LI Rui, ZHAO Tianjie, Vivien Stefan, GAO Qi	Giovanni Paolini

2.2. Description and Summary Table of EO and Other Data Utilized

An inventory of data used by each investigator and sub-project has been completed and the outcome of the inventory is presented in Table 2.

Table 2. Overview of data used in this project.

ESA Third Party Mission	Nr. of Scenes	ESA, Explorers and Sentinels Data	Nr. of Scenes	Chinese EO Data	Nr. of Scenes
ESA–CCI soil moisture products	910	Sentinel-1	120	ZY-3 TLA stereo images	14
ESA–CCI land cover	1	Sentinel-2	233	FY3-B/C SSM products	1920
L5/TM	29	Sentinel-3	200	GF-1	60
		SMOS	150	GF-2	50
		ESA 1 km LAI products	324	GF-3	1
				GF-5	1
Total	940		1027		

3. Subprojects Research and Approach

3.1. Satellite Data Products on Each Component of the Terrestrial Water Cycle at the Land–Atmosphere Interface

3.1.1. Research Aims

Multiple specific questions require urgent attention. Are current observations sufficient to characterize alpine glaciers and their changes? Will expected developments in sensor systems provide reliable measurements of snow water equivalent? Has the time come to build upon the body of knowledge on the land surface energy balance toward a better understanding of radiative and heat exchanges of glaciers and frozen ground with the atmosphere?

The aim of this sub-project was to help develop a suite of satellite observations and data products toward better cryosphere and hydrosphere science in cold, high elevation regions. Likewise, we expected to help identifying specific gaps in current observations and ways and means to fill such gaps. The cold-high elevation regions of China and particularly the Qinghai–Tibet Plateau is an ideal exploration and learning ground for the challenges outlined above.

3.1.2. Research Approach

WP1 Retrieval of Precipitation and Data Products

The research effort focused on the improvement and development of algorithms to retrieve total precipitable water of the atmospheric column using microwave radiometry.

WP2 Retrieval of Evaporation, Transpiration and Sublimation; Data Products

The ETMonitor system to retrieve water losses at the land surface was improved to deal with snow and ice. The set of surface biophysical and hydrological variables initially used as input was augmented to deal with sublimation. The ETMonitor model combines different ET parameterizations for different land cover types. Different procedures have been developed to deal with evaporation, including water intercepted by canopies, transpiration and different modules were integrated for each ET component. The improvement of ETMonitor was mainly focused on the following:

- Rainfall interception and evaporation;
- Root zone soil moisture;
- Snow and ice sublimation;
- Open water evaporation.

WP3 Retrieval of Biophysical Variables and Data Products

Land cover mapping. The Land Use and Cover Mapping Method (LUCMM) proposed by Zhong et al. [6] was used to map land cover at and around the test sites. Data including MODIS, HJ-1/CCD, and Landsat/TM and Google Earth images were used.

Compared to single classifier, multiple classifiers were integrated in LUCMM, including thresholding, Support Vector Machine (SVM), object-based method, and time series analysis to improve the accuracy of classification.

Leaf Area Index (LAI). The current retrieval algorithms implemented in our multi-source retrieval system was improved by combining radiometric data acquired by multiple sensors onboard European and Chinese satellites to achieve a better temporal and angular sampling. LAI products at 30 m and 1 km spatial resolution were generated to support hydrological research, particularly as input to ETMonitor.

Albedo. As with other land surface variables, both temporal sampling and accuracy was improved by combining radiometric data acquired by multiple sensors. This is particularly important to retrieve accurate albedo, which requires good angular and spectral sampling. The method to correct bi-conical reflectance measurements for anisotropy was improved.

WP4 Retrieval of Snow, Ice and Frozen Ground Variables and Data Products

Surface Soil Moisture (SSM) and freeze/thaw state. Both SSM and freeze/thaw state are best detected using microwave radiometry. We addressed ambiguities in microwave emittance and the effect of vegetation by using SAR and multispectral image data, The SAR image data were used to downscale the microwave radiometer data. We used the data acquired by SMOS, Sentinel-1 and FY-3.

Snow Cover Area (SCA) and Snow Water Equivalent (SWE). We generated a combined snow cover–snow water equivalent data product by using optical and microwave radiometric data. The multi-spectral image data acquired by Sentinel 2 and 3 and FY2 and 3, particularly by FY3/MWRI (Micro-WaveRadiation Imager) were used to estimate the SWE. The approach developed by Wang et al. [7] based on FY3/MWRI. could be improved by using Sentinel-1 SAR data, to discriminate wet snow cover. The proposed synergy of satellite passive and active microwave measurements is an improved approach to map and monitor snowpack properties.

Glaciers. We focused on analyzing changes in glaciers and coupled lakes. A new automatic glacier mapping algorithm was developed and applied by taking advantage of Landsat, HJ-CCD, and GF observations. The outline of clear ice and glacier lakes was extracted based on spectral index and surface properties. Debris cover was also detected by the combination of thermal infrared band and SAR images. We have also estimated glacier mass balance by using high resolution stereo-images and glacier surface velocity using multi-spectral images at moderate spatial resolution. The required data include HJ-CCD, S2/MSI, ZY-3, GF-1/2, and GF-3/SAR, ALOS-PALSAR and Sentinel-1/Interferometric Wide swath (S1/IW).

WP5 Retrieval of Extent of Water Bodies

Mapping and monitoring of water bodies will be improved combining multi-spectral and SAR satellite data. A machine learning method was used, after building a sample library of various type of water. Ancillary land cover data were used to resolve ambiguities in the delineation, as for example due to ephemeral aquatic vegetation. Empirical Mode Decomposition (EMD) was used to characterize the dynamics of inland surface water bodies.

WP6 Validation of Data Products

The data products were evaluated in four different ways: (a) comparison of data products on the same variable but were obtained with different algorithms; (b) airborne campaigns; (c) field experiments (e.g., HIWATER); (d) permanent observatories, e.g., on the Qinghai Tibet Plateau by ITP-CAS and CAREERI-CAS.

3.2. Observation and Modeling of High Elevation Hydrological Processes, including Accumulation and Ablation in Glaciers

3.2.1. Research Aims

The main goal of this sub-project was to unravel the hydrological functioning of representative high elevation glacierized catchments across the Tibetan Plateau and identify the causes for different glacier retreat rates and contribution to basin runoff in individual climate regimes. For this, we identified five specific objectives:

1. Advance our understanding of climate dynamics at high altitude and of precipitation patterns in particular;
2. Understand snow contribution to glacier mass balance and runoff and the main mechanisms of its redistribution and variability at the catchment scale;
3. Investigate the role played by debris cover on the mass balance of glaciers, thus contributing to solving the so-called debris-cover "anomaly" that has suggested high rates of mass loss for these glaciers despite the assumed insulating effect of debris;
4. Understand the energy and mass balance of glaciers in the TP and their changes in different climate regions, through development of a physically based mass balance model;
5. Quantify snow and glacier contribution to total catchment runoff and assess regional differences in catchment hydrology by incorporating knowledge of physical processes into an integrated modeling approach that includes all relevant processes responsible for runoff generation, their interconnection and their spatial and temporal variability.

3.2.2. Research Approach

To achieve the objectives above, we use a combination of techniques and approaches: remote sensing, field work and modeling at different scales, from the point-scale location of Automatic Weather Stations (AWSs) to the glacier and catchment scale of the glacio-hydrological model. Our research is organized around five main work packages (WPs), in which we: (i) provide an advanced characterization of the climatic drivers in high elevation catchments of the Tibetan Plateau; (ii) collect datasets for processes under-represented in HMA and still poorly understood, including snow processes and the dynamics of debris-covered glaciers; (iii) develop a physically based energy balance model of glacier changes based on work undertaken by both PIs; and (iv) include knowledge of physical processes in a distributed hydrological model which represents the complexity of catchment response with an enhanced physical basis for greater robustness and transferability. The distributed hydrological model is then used to quantify the spatial distribution, seasonality and interannual variability of snow and glacier contributions to runoff.

WP1 is designed to advance understanding of the regional climate drivers of the basin's hydrology, by analyzing satellite observations together with ground meteorological data using the temperature models and extrapolation techniques developed by the PI. WP2 exploits remotely sensed datasets of snow characteristics to understand snow processes. WP3 is designed to progress understanding of processes in debris-covered glaciers, their mass balance and role in catchment hydrology, with a special focus on the role of supra-glacial cliffs and lakes. WP4 integrates new knowledge on snow and ice processes into a physically based energy and mass balance model of both debris-covered and debris-free glaciers to study glacier mass balance patterns in time and space. Finally, WP5 incorporates knowledge gained in WP2, WP3 and WP4 into a state-of-the-art glacio-hydrological model for simulations of the hydrology of high elevation catchments in the Tibetan Plateau, integrating the project scientific findings into a coherent and novel modeling chain.

The study sites chosen are Parlung No. 4 Glacier and 24 K Glacier (maritime glaciers, the latter covered by debris) in the Tibetan Plateau, and the Langtang Glacier in the Nepalese Himalaya. They all had existing glaciological and hydrological observations led by the Chinese and European PIs respectively, and we have carried out additional field campaigns since the start of this project. While Parlung No. 4 Glacier and 24 K Glacier are located in the same broad climatic region, one glacier is debris covered, and one is

debris free. Langtang glacier and its catchment on the other side, is located in a distinct climatic setting, and the combination of the three sites is ideal to investigate the complexity of interlinked processes typical of catchments in the TP.

3.3. Forcing, Calibration, Validation and Data Assimilation in Basin Scale Hydrological Models Using Satellite Data Products

3.3.1. Research Aims

The main objective of this project was to improve the estimate of water balance under natural and human pressure on the Heihe river basin in China and in the Po river basin in Italy, by using MOST, ESA, Third Party Mission and NASA satellite data coupled with three distributed hydrological models (FEST-EWB, SHAW-DBHM, HeiFLOW). This was to be achieved simulating ET, SSM, discharge, SWE and groundwater dynamic at different spatial and temporal scales. This approach can fill the gap between quantitative hydrology and remote sensing information. Multi-source remote sensing data, from visible to thermal infrared and microwave, were used for forcing, calibration, validation and data assimilation of/into basin scale hydrological models. Vegetation parameters, snow coverage, LST and soil water content, lakes extent and water level height, and meteorological forcing were retrieved.

3.3.2. Research Approach

The study focused on two river basins: Chiese in Northern Italy and Heihe in Gansu, China.

The project is subdivided in four work packages (WP) which correspond to each objective. Each WP is now described separately.

WP1: Satellite Data on Land Surface Properties for Hydrological Modeling

Remotely sensed products at different temporal and spatial resolution of parameters Leaf Area Index (LAI), Fractional Coverage of Vegetation (FCV) and albedo, were used as inputs to hydrological models. Retrievals of model state variables, SSM, ET. LST, snow coverage, SWE, river and lake height, by using both European and Chinese satellites were applied for data assimilation and model evaluation. The temporal resolution and the spatial information provided by satellite data allowed monitoring over time in all the investigated case studies. Implementation of a database of meteorological and hydrological data from satellite and ground information supported this research effort.

For both case studies LST data were obtained from MODIS LST/Emissivity (E) Daily L3 Global 1 km Grid product (MOD11A1) with a spatial resolution of 1 km and a daily temporal resolution and were used (http://ladsweb.nascom.nasa.gov/index.html, accessed on 13 October 2021) for model calibration. Vegetation parameters (e.g., vegetation fraction and LAI) and albedo were obtained by merging MODIS data MOD15A2–leaf area index at 500 m spatial resolution and Sentinel 2 data at 10 m and Landsat 8 at 30 m.

WP2: Database of Hydro Meteorological Forcings

Meteorological data are needed for running the hydrological models. These included incoming shortwave radiation, air temperature and relative humidity, wind speed and precipitation. These were collected from available ground network in each area of study. In the Chiese basin, meteorological data are collected at 22 stations of the national measuring network managed by ARPA Lombardia and Regione Trentino, which also provide river discharge data at four river cross sections. Eddy covariance data were also available from 2016 to 2018 in a maize field. Moreover, due to unavailability in some areas, meteorological forcing was gap-filled by combining ground and remote sensing information. Hence, high resolution forcing datasets were obtained by applying a dynamic and statistical downscaling algorithm, which assimilates Tropical Rainfall Measuring Mission (TRMM) and FY remote sensing precipitation products into the Weather Research and Forecasting

(WRF) model [8]. Ground hydrological data on discharge, ET and SSM, when available, were used for calibration and validation of hydrological models.

WP3: Hydrological Modeling: Calibration/Validation

Calibration/validation of hydrological water balance models for water resources assessment was performed using satellite data on land surface temperature, soil moisture and snow cover in combination with ground data. Three distributed hydrological models were used in the different case study areas. The hydrological models are innovative due to the use of satellite data for parameterization, validation and improvement. These models are based on different modeling hypotheses, remote sensing input data and calibration methodologies.

The FEST-EWB distributed hydrological model [9], with its energy–water balance scheme, allows to compute continuously in time and distributed in space both SSM and ET. The model is part of the effort toward integrating and assimilating remote sensing data products into hydrological modeling, both as input parameters (e.g., Leaf Area Index) and as variables for model state up-date (such as Land Surface Temperature, LST). This LST-oriented approach solves most of the problems of the actual ET and SSM computation, contributing to the closure of both the energy and water balance. The integration of the remote sensing data into the model allows a pixel wise calibration of the hydrological model minimizing the differences between the satellite LST and the FEST EWB simulated surface temperature, also defined as RET (representative equilibrium temperature) for its physical meaning. The sensitivity analysis performed at local scale using eddy covariance data suggests that the main surface parameters to be tuned are: soil hydraulic conductivity, Brooks–Corey index, soil depth, minimum stomatal and soil resistances. The FEST-EWB model computes also runoff routing throughout the hillslope and the river network via a diffusion wave scheme based on the Muskingum–Cunge method in its non-linear form with the time variable celerity. Runoff is computed according to a modified SCS-CN method extended for continuous simulation [10]. The subsurface flow routing is computed with a linear reservoir routing scheme. The model flow routing parameters are calibrated with a more traditional discharge-oriented approach, featuring both superficial and subsurface discharges calibrated with point-wise discharge measurements [11]. The calibration of snow accumulation and melt parameters is described in Corbari et al. [12].

WP4: Operational Hydrological Data Products

Monitoring of water cycle components was performed with remote sensing data and the hydrological model at high spatial and temporal resolutions, providing high quality datasets. The calibrated and validated hydrological models coupled with satellite data provided consistent outputs on the different hydrological processes overcoming the limitation of remote sensing data caused by cloud cover, retrieval algorithms, temporal and spatial resolutions, etc. In particular, for the different case studies, SSM, ET, ground water dynamic, and SWE datasets were computed. Moreover, flow duration curves and discharges for different rivers cross sections were computed.

3.4. Monitoring Water Resources in Red River Basin Using Microwave Remote Sensing

3.4.1. Research Aims

The main scientific objective of this project was to develop the algorithms and synergies between different Microwave Remote Sensing sensors to be able to monitor water resources in the Red River Basin.

The results of this project can play a key role in improving the knowledge on water stocks and exchanges in large regions. The potential applications are many, and most of them have strong political and strategic implications:

- Determining the water balance of a region;
- Determining the agricultural water balance;
- Mitigating and predicting flood, landslide and drought risk;

- Designing irrigation schemes and managing agricultural productivity;
- Predicting geomorphological changes, such as erosion or sedimentation;
- Assessing the impacts of natural and anthropogenic environmental change on water resources.

The project, at the same time, aimed at building a network for knowledge sharing and long-term collaboration in the field of microwave remote sensing for water resources management. The project builds on existing or completed projects and some of the partners have already collaborated in international projects.

3.4.2. Research Approach

This project not only intended to make the best use of all recent improvements in altimetry and microwave remote sensing but also pushed for synergies that may boost the scientific and operational use of microwave data in hydrology.

Space borne radar altimetry offers an efficient way to yield hydrological information due to its global coverage and systematic revisit. Several hydrology data products can be derived from altimetry: for lake and wetlands water surface elevation changes and water flow discharge for rivers. Satellite radar altimetry has effectively been used for monitoring water surface elevation changes. Current water level products such as the ESA Rivers and Lakes (http://tethys.eaprs.cse.dmu.ac.uk/RiverLake/shared/main, accessed on 13 October 2021), the DAHITI service (http://dahiti.dgfi.tum.de/, accessed on 13 October 2021), or the hydroweb (http://www.legos.obs-mip.fr/en/soa/hydrologie/hydroweb/, accessed on 13 October 2021), provide quality and useful information but somewhat delayed and cover only partially the area of interest. In particular, the Red River basin, which is not covered by any of these services, was studied in this sub-project.

Although nadir radar altimetry has been used to provide estimates of water level in rivers and lakes all over the world, none of the altimetry missions used to date were tuned for continental waters. The major drawback of radar altimetry is the several kilometer-wide footprint. In such a footprint, energy bounced back by non-water reflectors is polluting the echo received by the satellite antenna, making it difficult to estimate the level of the water body included in the footprint.

Consequently, until now, it has been possible to monitor only rivers and lakes with large extension using measurements from their central part where a "clean" return from the water body could be expected.

Recent technological development has allowed the development of SAR altimeters. This concept has been tested on CryoSat-2 and has been also implemented on the operational Sentinel-3. Thanks to SAR altimetry, the slicing of the altimeter footprint that the SAR mode performs, allows the separate computation of all the elementary reflectors, in particular the wet ones.

In this project, we will take advantage of Radar Altimetry (RA) to monitor smaller water bodies in the Red River basin as an extension of our Dragon-3 project (prj. Nr. 10,466 applications of radar altimeter data) and will improve the L1 and L2 algorithms in the altimetry processing chain for higher precision data products.

Hydrological help solving many practical problems in environmental engineering, flood protection and understanding water cycle processes and water balance. The Soil and Water Assessment Tool (SWAT) is a small watershed to river basin-scale model used to simulate the quality and quantity of surface and ground water and predict the environmental impact of land use, land management practices and climate change (https://swat.tamu.edu/, accessed on 13 October 2021). However, there are several uncertainties due to complex landscape, shortage of ground meteorological observations and so on. This applies specifically to the upstream area of the Red River Basin, because of its complex geographical environment such as mountainous area, dry valleys, terrace and karst landform. Spaceborne microwave precipitation retrievals could be a practical data source for hydrological modeling. In this project, we simulated runoff and cross validated the results by monitoring water bodies with radar altimetry.

4. Research Results and Conclusions

4.1. Satellite Data Products on Each Component of the Terrestrial Water Cycle at the Land–Atmosphere Interface

4.1.1. Results

Quantitative information on water loss is important to understand the global terrestrial water cycle and land–atmosphere interactions. However, land surface water loss (i.e., ET) estimated by land surface models usually neglects the sub-grid heterogeneity of land atmosphere properties, and it will cause aggregation biases in spatially averaged ET estimates, considering the nonlinear dependence of ET on the heterogeneous land-atmosphere properties. One frequently adopted strategy clusters the heterogeneous surface within a model grid into several tiles, assumed to be homogeneous, usually based on high-resolution land cover data. While the differences in bulk-averaged parameters between different tiles are considered, the heterogeneity within each tile is neglected. The response of ET to changes in SSM or LAI generally can have three forms (see Figure 2). To evaluate the aggregation bias, a numerical analysis was conducted to compare the ET estimates based on bulk-averaged SSM and LAI with the one obtained by aggregation of the flux estimates based on the Probability Distribution Function (PDF), which complies with energy conservation [13]. Four types of PDF were used to simulate different scenarios on the heterogeneity (within a tile) of SSM and LAI, i.e., from water scarcity to wet, and from sparse to dense vegetation covered surfaces. Overall, the numerical experiments indicated that impacts on tile ET related to LAI are smaller than the ones related to SSM. Different meteorological conditions combined with the nonlinear dependence of ET on SSM/LAI may lead to large changes in the aggregation bias, from underestimates to overestimates or conversely. In climate conditions with larger atmospheric water demand enhancing evaporation, underestimation is more likely, and vice versa. Neglecting the actual spatial variability of both SSM and LAI within tiles can lead to both large relative error (>20%) and absolute error (>1 mm/day) in the estimated ET in semi-arid areas. A negative bias is expected at low ET/ET0, and a positive bias is expected at large ET/ET0, regardless of climate conditions (i.e., ET0). The relation between aggregation bias and meteorology found in this study has the potential to identify or even as a starting point to correct the possible serious underestimations and overestimations in applications.

ET is a key terrestrial water cycle element at the land-atmosphere interface, and the earth observation are expected to provide spatially and temporally continuous information on large scale ET variability. The ETMonitor model combines different ET parameterizations for different land cover types. Different procedures have been developed to deal with evaporation, including of water intercepted by canopies, transpiration and different modules were integrated for each ET component. The ETMonitor system to retrieve water losses at the land surface was improved to deal with rainfall interception loss, and snow and ice sublimation. The set of surface biophysical and hydrological variables currently used as input will be augmented to deal with sublimation. The analytical Gash model was adapted and applied in ETMonitor to estimate rainfall interception loss, on the basis of satellite remote sensing products, for example, gross rainfall amount and rate and leaf area index [14]. The Penman–Monteith equation-based snow/ice sublimation, which is evaluated with bulk aerodynamic method and eddy covariance system observation in Wang et al. [15], was adopted in ETMonitor for snow/ice sublimation estimation. The improved ETMonitor was applied to estimate total ET and its components at high resolution (1 km), with a suit of relevant surface biophysical and hydrological variables as input, including the land cover, land surface temperature, leaf area index, albedo, soil moisture, and so on. The ETMonitor was used to estimate ET in the HMA with daily interval and 1 km resolution from 2000–2018. The ET estimation adopted the ESA–CCI (European Space Agency–Climate Change Initiative) soil moisture data product as downscaled to 1 km resolution as one of the key inputs. The estimated ET generally capture the spatial pattern of ET (Figure 3a). To evaluate the accuracy of the estimated ET by ETMonitor, we collectedobservations of latent heat flux by the eddy covariance system from 10 flux

tower sites in this region provided by Heihe watershed allied telemetry experimental research (HiWATER) [16] and the land–atmosphere interaction observations on the Tibetan Plateau [17]. The quality of collected latent heat flux at 30 min interval was carefully checked to obtain the in situ daily ET. Generally, the estimated daily ET by ETMonitor agreed well with the in situ observations at site scale in the HMA region, with overall high correlation (0.83), low bias (0.16 mm d^{-1}), and low root mean square error (0.74 mm d^{-1}) (Figure 3a,b). The estimated ET time series in the HMA region could capture the expected ET patterns both in space and in time (Figure 3c). Further effort is ongoing to generate global ET dataset to document broader characteristics and applications ET as indicated by Jia et al. [18].

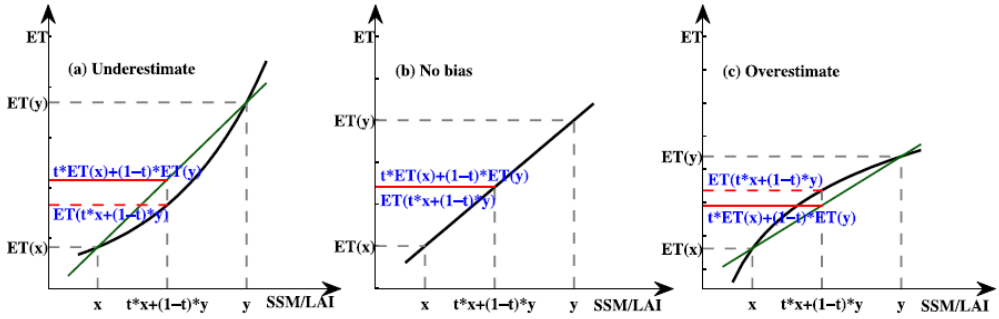

Figure 2. Conceptual diagram of the response modes of ET to SSM or LAI and the corresponding aggregation bias. (**a**) Convex downward response which induces underestimation if areal averaged parameter is adopted; (**b**) linear response without bias; (**c**) concave downward response (adapted from Chen et al. [13]).

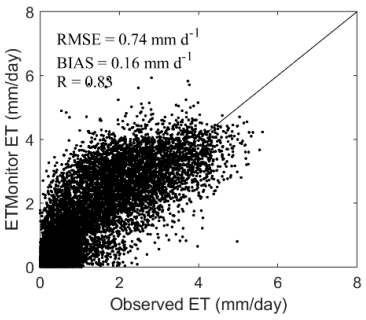

(**a**) Scatterplot to compare ETMonitor estimated ET with 10 flux towers observation in the HMA.

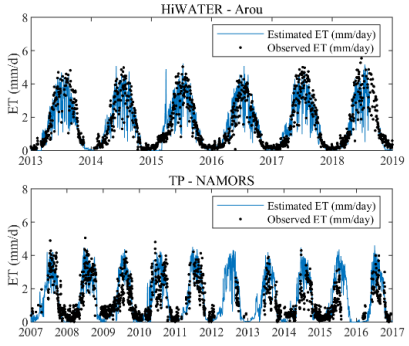

(**b**) Example of estimated ET time series at 2 typical flux towers in the HMA.

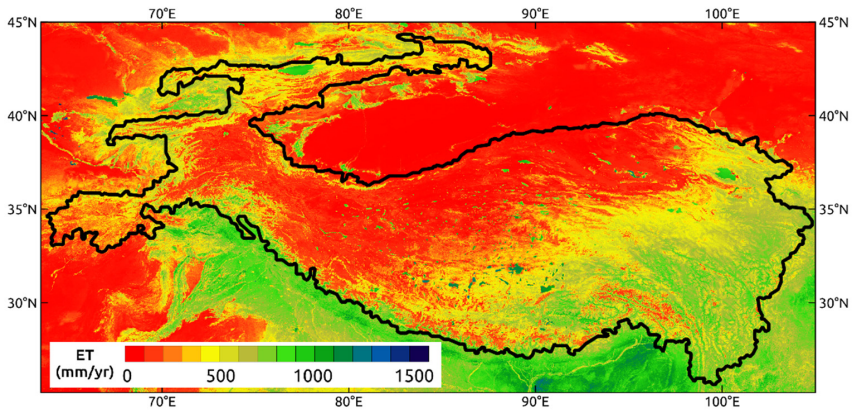

(**c**) Spatial pattern of multi-year averaged ET (2000–2018) in High Mountain Asia region

Figure 3. (**a**,**b**) Comparison of ET estimated by ETMonitor with ground measurements of flux data in HMA and (**c**) spatial pattern of ET from ETMonitor in the HMA region.

In the context of global climate change, the glaciers of the Tibet Plateau are undergoing significant change, which plays an important role in the study of the interaction between the plateau and the earth–atmosphere system. Based on the Chinese and European satellites, the project has carried out the mapping of typical glacial area and glacier mass balance of the Tibetan Plateau. An optimized procedure was developed to retrieve glacier mass balance by combing the Chinese high spatial resolution ZY-3 Three-Line-Array (TLA) stereo images and C-band Shuttle Radar Topography Mission (SRTM) Digital Elevation Model (DEM) [19]. Using the new developed procedure, ZY-3 TLA data can significantly increase point cloud density and decrease invalid data on the glacier surface to generate a high resolution (5 m) glacier mass balance map. The glacier mass balance in the Nyainqentanglha Mountains (NM) region from 2000 to 2017 were obtained accordingly (Figure 4). The glacier mass balance in both the Western and Eastern NM (WNM and ENM) was negative in 2000–2017 and experienced faster mass loss in recent years (2013–2017) in the WNM. Overall, the glaciers in the WNMand ENM show different change patterns since they are influenced by different climate regimes; the glacier mass balances in WNM region were -0.22 ± 0.23 and -0.48 ± 0.06 m w.e. a^{-1} in 2000–2013 and 2013–2017, respectively, while in 2000–2017, it was -0.30 ± 0.19 m w.e. a^{-1} in the WNM region and –0.56 $\pm$ 0.20 m w.e. a^{-1} in the ENM region. In the WNM region, the glaciers experienced mass loss in 2000–2013 and 2013–2017 in the ablation zone, while in the accumulation zone mass increased in 2000–2013 and a large mass loss occurred in 2013–2017; as regards the ENM region, the glacier mass balance was negative in 2000–2017 in both zones.

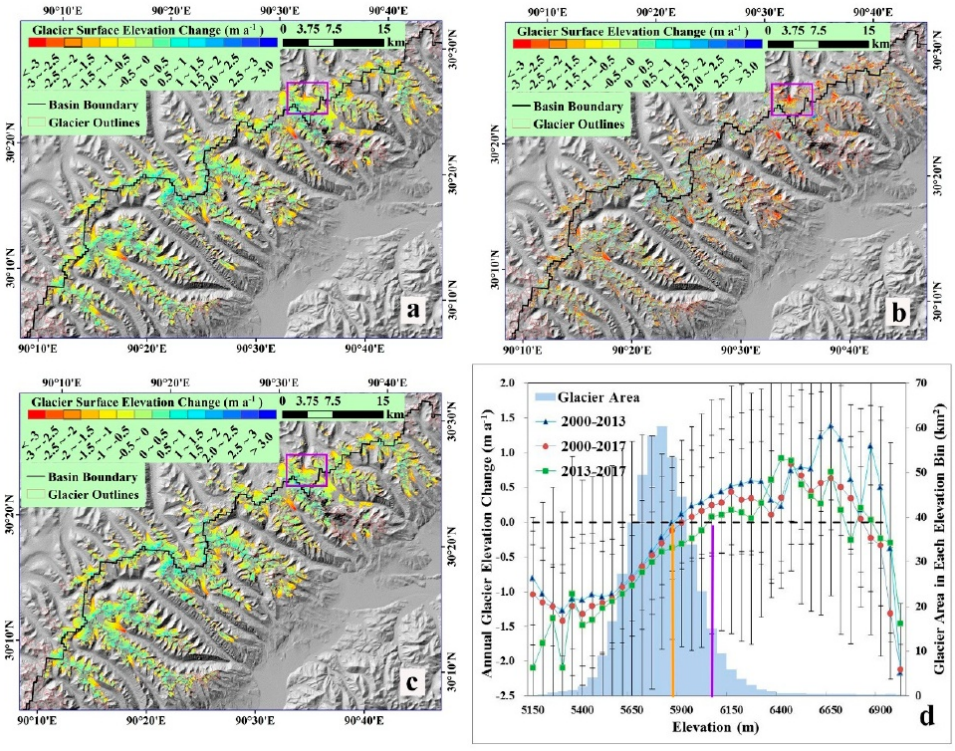

Figure 4. Annual glacier elevation changes in the WNM. (**a**) 2000–2013; (**b**) 2013–2017; (**c**) 2000–2017; (**d**) annual glacier elevation change versus elevation (the dotted black line is the zero mass balance line, the orange and purple solid vertical lines represent the equilibrium line altitude (ELA) lines in the 2000–2013 and 2013–2017, respectively); adapted from [19].

We investigated the glacier surface velocity in the Parlung Zangbo Basin (PZB) by applying the normalized image cross-correlation method to S2/MSI and LL8/OLI image data acquired from 2013 to 2020 (Figure 5) [20]. We mapped time-averaged glacier surface velocity and examined four typical glaciers (Yanong, Parlung No. 4, Xueyougu and Azha)

in the PZB. We explored the driving factors of surface velocity and of its spatial and temporal variability. The analysis of seasonal velocities in the Yanong, Parlung No. 4, Azha, and Xueyougu Glaciers revealed additional insights on temporal and spatial changes (Figure 5).

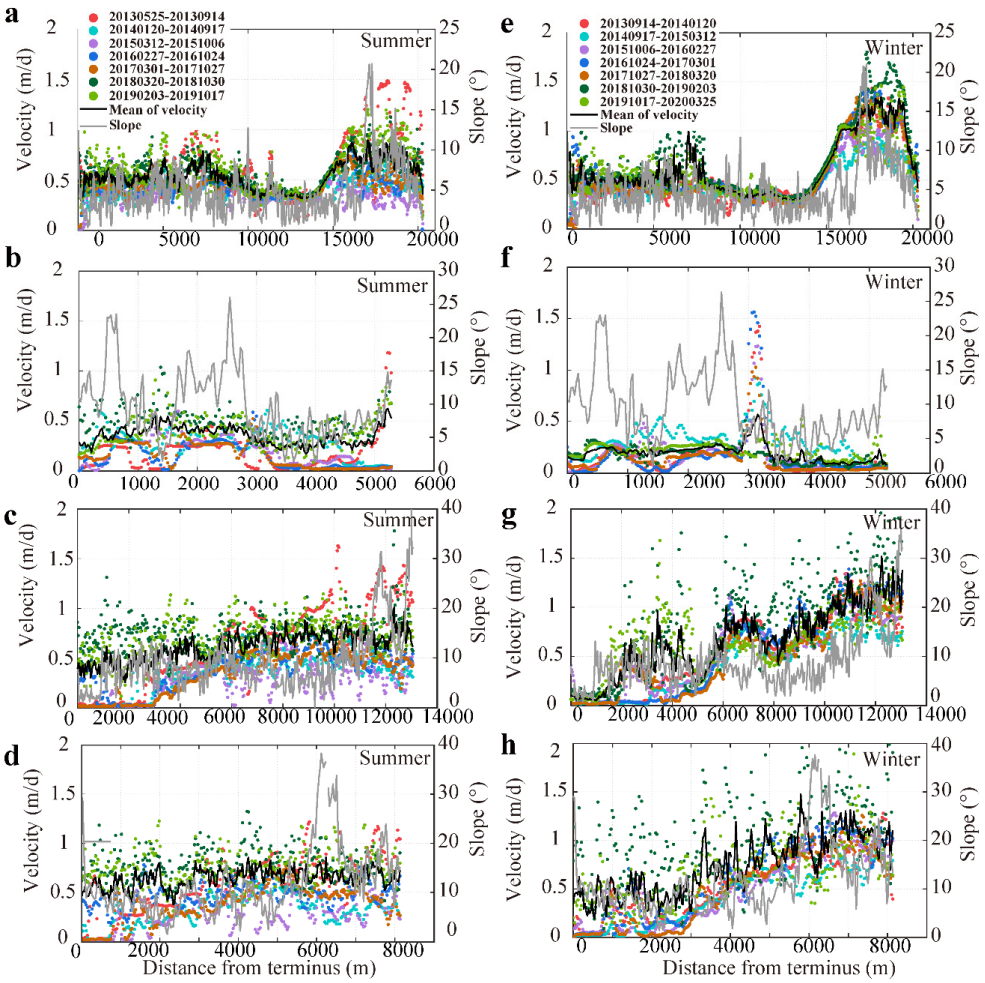

Figure 5. Summer (left, 2013–2019) and winter (right, 2013–2020) center flowline velocities vs. distance from terminus: Yanong Glacier (**a**,**e**) (GLIMS ID G096657E29334N); Parlung No. 4 Glacier (**b**,**f**) (GLIMS ID G096920E29228N); Azha (**c**,**g**) (GLIMS ID G096818E29132N) and Xueyougu Glacier (**d**,**h**) (GLIMS ID G096758E29147N); mean velocity (black solid line); adapted from Zhang et al. [20].

Summer and winter velocities for seven years, i.e., from 2013 till 2020, were also retrieved for the Parlung No. 4 Glacier (Figure 5b,f). Overall, differences between summer and winter were smaller than the ones observed in the other glaciers. Compared with the other glaciers, Parlung No. 4 Glacier is characterized by a smaller range in elevation and by slope being higher and more variable near the terminus (Figure 5b,f). Some fluctuations in the mean velocity were observed, especially in summer and closer to the terminus, i.e., up to 2000 m, with a summer mean velocity of 0.5 m/d. The mean winter velocity shows a peak up to 1.5 m/d between 3000 and 3200 m where interannual variability is large.

We have improved and evaluated a method to correct glacier and snow reflectance for anisotropy and retrieve better albedo (hemispherical reflectance) [21]. The anisotropy correction was developed using airborne directional measurements of spectral reflectance and comparing alternate parameterizations [21]. This method was applied to retrieve glacier albedo in the entire WNM using MODIS data for the period 2001–2020 (Figure 6).

There is significant spatial variability in albedo within a glacier, as shown for the Parlung No. 4 Glacier in Figure 5b, which implies a significant spatial variability in net

radiation and energy balance. The spatial resolution of OLI (Figure 6b) seems sufficient to capture the spatial details observed by S2/MSI (Figure 6a). The albedo of the entire WNM region, particularly of snow and ice, is clearly decreasing (Figure 6c), leading to a steady increase in radiative forcing of glacier melt. The actual impact on glacier mass balance needs to be evaluated in detail by means of numerical experiments with distributed models of energy and mass transfer at the surface of and within a glacier and snowpack.

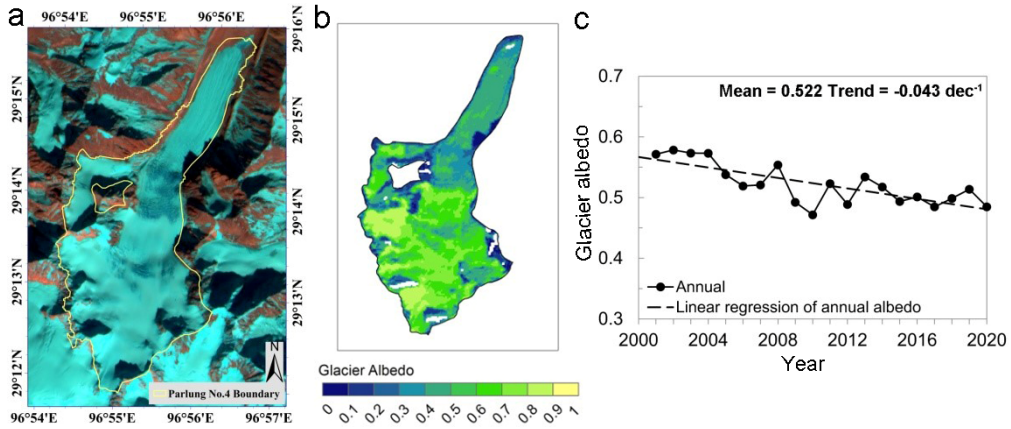

Figure 6. Glacier albedo in the Nyainqentanglha Mountains: (**a**) Parlung No. 4 Glacier S2/MSI colour composite (red, band 11; green, band 8; blue, band 4) 7 December 2017; (**b**) Parlung No. 4 Glacier albedo derive by our method using OLI data on 6 December 2014 (adapted from Ren et al. [21]); (**c**) mean annual albedo in the WNM derived by our method using MODIS data 2001–2020.

4.1.2. Conclusions

The efforts invested in improving and extending the algorithms and data products available at project inception were successful to a large extent. Particularly, the ETMonitor system, originally designed and developed to deal with hydrological processes characteristic of alluvial plains, was extended to deal with high elevation, cold regions. The system can now generate time series of data products on snow and ice sublimation across a range of spatial resolutions. Studies on the observation of glacier were rather comprehensive and focused particularly on glacier albedo, which controls radiative forcing of glacier mass balance and the coupling of the cryosphere with the atmosphere. We also achieved good progress in observing the glacier mass balance with stereo-images at high spatial resolution and the response of glacier surface flow to the spatial and temporal variability of the mass balance. The information captured in this way leads to the usage of remote sensing higher level data products in distributed models of glaciers (see Section 4.2).

4.2. Observation and Modeling of High Elevation Hydrological Processes, including Accumulation and Ablation in Glaciers

4.2.1. Results

Observation and Modeling of Glacier Energy and Mass Balance

Observations of the glacier energy and mass balance are important to understand glacier surface processes (see also Section 4.1.1). The field experiment on the Parlung No. 4 Glacier in the southeast Tibetan Plateau, a debris-free glacier, has been initiated in 2009 by the Institute of Tibetan Plateau Research, Chinese Academy of Sciences. Meteorological and radiation data have been collected, such as surface air temperature, relative humidity, wind speed, air pressure, precipitation, solar and longwave radiation. A broadly similar experiment is being carried out at the debris-covered 24 K Glacier. Besides the meteorological data and glacier ablation stakes, UAV equipped with a GPS system was used to measure the glacier surface elevation and to obtain high-accuracy orthophoto images and DEM data in August and October in 2020. A set of radar level gauge was set up at

3800 m a.s.l. to obtain the change of water level at the terminus of the glacier and another one at 2800 m a.s.l. to monitor the runoff water level of the whole basin.

The Water and Enthalpy Budget-based Glacier mass balance Model (WEB-GM) was developed and used to simulate the glacier surface energy budget and mass balance [22]. In this model, enthalpy (H), rather than temperature, is used as a state variable of the glacier and snow layers. The enthalpy of liquid water at freezing point is set at zero, such that the computation of energy flow through liquid water movement and phase transition can be simplified. The model has been developed as a distributed model, in which a data preparation module deals with the DEM and glacier inventory information, while parameterizations are applied to generate distributed input meteorological and radiation data. Initial conditions for the snow and ice layers need to be estimated.

This distributed glacier mass balance model has been applied to study the mass-balance of the Parlung No. 4 Glacier during 24 May to 28 August 2009. The spatial resolution was 150 m and time step 1 h.

The model estimates (Figure 7) show that the accumulated glacier melt during the whole period was about 1.5 to 2.5 m w.e. in the accumulation zone of the Parlung No. 4 Glacier, and about 4.5 to 6.0 m w.e. in the ablation zone, reaching 6.5 m w.e. at the terminus. Melting mainly occurs in June and July on the Parlung No. 4 Glacier, more precisely in the accumulation zone it is similar in June and July, while in the ablation zone the melting in July is much more than that in June.

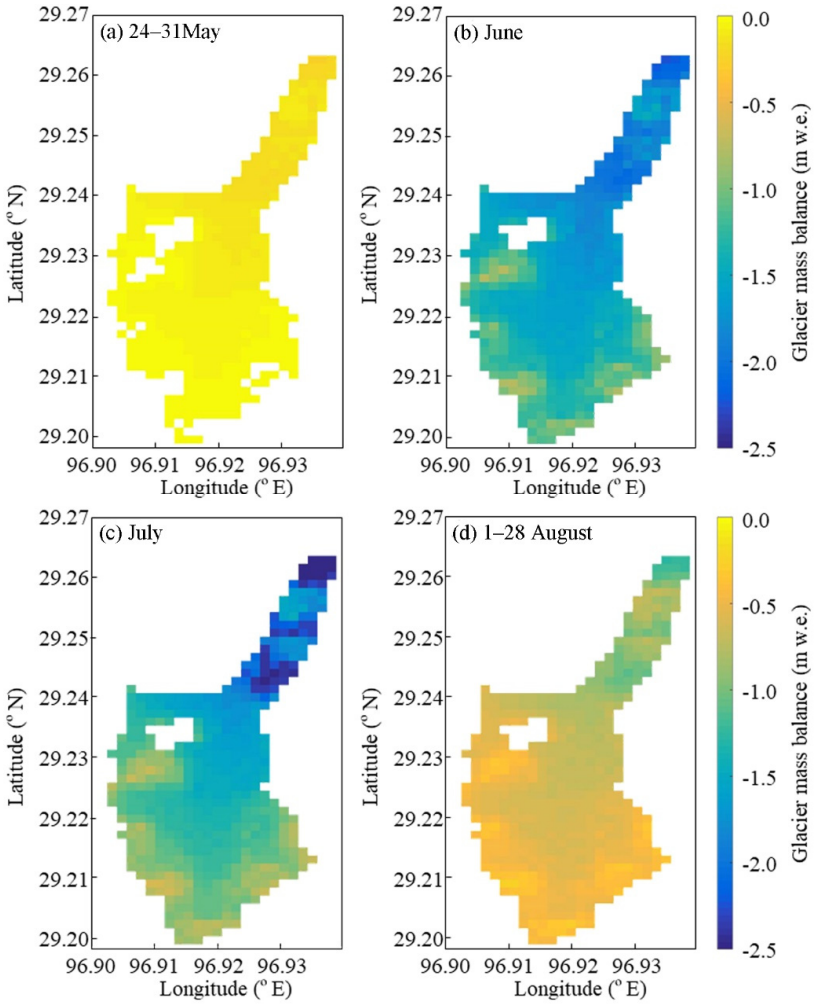

Figure 7. Monthly glacier mass balance (m w.e.) during 24 May to 28 August 2009 at the Parlung No. 4 Glacier. (**a**) 24–31 May; (**b**) June; (**c**) July; (**d**) 1–28 August.

Advance our understanding of climate dynamics at high altitude and of precipitation patterns in particular.

Our analysis of near-surface air temperature in glacierized catchments of S and E Tibetan Plateau [23] highlighted the glacier size-dependence of boundary layer modifications due to glacier cooling, with a strong decrease in on-glacier temperature sensitivity to off-glacier temperatures for flowlines greater than 2 km, whereas small glaciers are highly sensitive to off-glacier air temperature patterns.

Our application of long-term high-resolution snowline mapping demonstrated for a monsoon-influenced catchment that snowline altitudes show seasonal aspect differentiation due to shortwave reception [24]. Snowline altitudes are seasonally controlled by distinct meteorological controls: precipitation in winter, net melt in pre-monsoon, a mixture in post-monsoon, and temperature alone in summer. We also revealed spatial gradients in precipitation within the high-elevation catchment.

Understand snow patterns and contribution to glacier mass balance and runoff and the main mechanisms of its redistribution and variability at the catchment scales.

The fine-scale understanding of snow cover dynamics at the catchment scale using the [24] approach was important for calibrating snow redistribution routines, while field measurements of glacier mass balance and river discharge were invaluable for model validation. These and additional remote sensing datasets were used to calculate through a glacio-hydrological model the snowmelt contribution to total catchment runoff for the case study catchment.

Investigate the role played by debris cover on the mass balance of glaciers, thus contributing to solving the so-called debris-covered "anomaly" that has suggested high rates of mass loss for these glaciers despite the assumed insulating effect of debris.

We quantified the state of the world's glaciers in terms of debris cover, highlighting HMA as being one of the regions with the highest proportion of debris on its glaciers and representing one third of all of Earth's on-glacier debris [25]. In addition, we found that, despite a large variability, on average HMA debris-covered glaciers were at more advanced stages than in other regions, and thus closer to reaching their full glacier carrying capacity [25]. We also quantified the cliff and pond distribution for a few debris-covered glaciers in Nepal (Khumbu and Langtang) and India (Satopanth) and found that cliffs (ponds) represented between 3% and 10% (1% and 3%) of the glaciers' debris-covered area [26–29]. Most importantly, we found that these supraglacial features displayed a high variability at the interannual scale [27,29] and even at the intra-annual scale for ponds [27]. For cliffs, we could demonstrate using a 3D energy-balance model that this variability was partly driven by their aspect, and that south-facing cliffs tended to become shallower and be reburied by debris within months while north-facing cliffs persisted [30]. These cliffs and ponds enhance melt relative to debris-covered ice and despite their low relative area, we have shown that they contribute to approximately one third (12.5 $\pm$ 2.0% for ponds, and 17 $\pm$ 4%) of the ice loss of the glaciers in Langtang catchment [31,32].

Understand the energy and mass balance of glaciers in the TP and their changes in different climate regions, through development of a physically based mass balance model.

The enthalpy-based mass balance model described above [22] showed excellent performance at Parlung No. 4 Glacier, while simultaneously improving computational efficiency. The adapted land-surface model has shown superb skill for modeling glacier energy balance for differing surface conditions varying from snow to bare ice, to surface dust or debris clasts (Figure 8) and clearly resolves the highly distinct energy fluxes and melt rates typical for glaciers with differing surface types in the same climatic setting. In particular, it is clear that debris cover beyond a critical thickness has an insulating effect on the glacier (e.g., 24 K Glacier with 20 cm debris thickness), with reduced melt-rates compared to the clean-ice glacier (Parlung No. 4), while thin debris cover (Hailuogou, 1 cm) has a melt-enhancing effect. There is also a difference between the signs of the turbulent heat fluxes (latent and sensible): While evaporation (removal of energy from the debris cover) occurs on the thick

debris (24 K), condensation (addition of energy to the glacier surface) is a more relevant process on both the clean ice and thinly debris-covered surfaces.

Quantify snow and glacier contribution to total catchment runoff and assess regional differences in catchment hydrology by incorporating knowledge of physical processes into an integrated modeling approach that includes all relevant processes responsible for runoff generation, their interconnection and their spatial and temporal variability.

The careful calibration of TOPKAPI-ETH at Parlung No. 4 resulted in a good agreement between the simulation results, the various in-situ datasets (discharge, stakes, albedo) and the observations derived from remote sensing (distributed elevation change, fractional snow cover). Over the 2000–2018 period, the annual mean discharge simulated at the catchment outlet amounted to 1.57 m^3 s^{-1}, out of which 25% and 23% flowed in July and August respectively, followed by June and September (19% both). Our simulations reveal that snowmelt represented the most important water input to the hydrological system, accounting for an annual mean ($\pm$ 1 std dev.) of 51 $\pm$ 4.4% of the total water input, followed by ice melt (27 $\pm$ 7%) and rain (22 $\pm$ 4%). Snow and glacier contribution to total catchment runoff varied through the year, initially originating mostly from snow-melt until mid-June, after which rain and ice melt started to noticeably contribute to catchment runoff (Figure 9c). Ice melt contribution reached a peak at the end of summer–beginning of autumn, when most of the seasonal snowpack had melted out and more areas of bare-ice were exposed to melt. The contribution of ice melt to total discharge showed the largest variability and was correlated (R^2 = 0.47) with spring precipitation amounts. The latter controls the seasonal snowpack thickness, which protects the underlying ice and reflects relatively more shortwave radiation, lowering the amount of energy available for melt and further delaying the bare-ice exposure. The different zones of the catchment generated varying amounts of glacier and snow melt depending to their elevation (Figure 9b). As it can be expected, most of the ice melt was generated near 4800 m a.s.l., which is close to the glacier terminus in the ablation zone, where are experienced the highest temperature and a concurrent rapid seasonal snowpack melt-out. Most of the snow-melt originated from the zones between 5200 and 5500 m a.s.l. for three reasons: (i) the catchment hypsometry shows the largest areas in this elevation band; (ii) there is a strong vertical precipitation gradient, leading to more precipitation falling there than near the glacier terminus; (iii) along with colder temperature, most of the precipitation fell as snowfall.

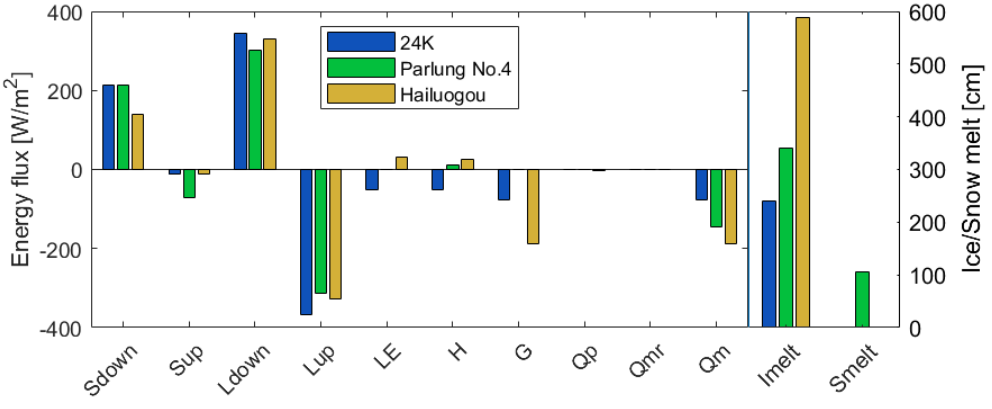

Figure 8. Mean energy fluxes over the period 1 June to 30 September 2016 (24 K, Parlung No. 4), and 2008 (Hailuogou). Incoming/outgoing shortwave radiation (S_{down}/S_{up}), incoming/outgoing longwave radiation (L_{down}/L_{up}), latent and sensible heat flux (LE and H), ground heat flux (G), precipitation advected heat flux, snowpack melt/refreeze energy (Q_{mr}), total melt energy (Q_m). Positive (negative) values indicate an energy flux toward (away) from the surface. Sums of ice and snow melt (I_{melt}, S_{melt}).

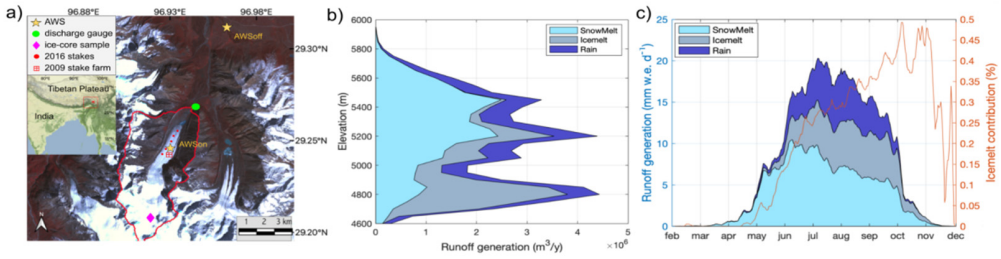

Figure 9. Glacio-hydrological modeling at Parlung No. 4 catchment. (**a**) Location map of catchment and instruments. (**b**) Annual run-off as a function of elevation (50 m elevation bands), averaged over the 2000–2018 period. (**c**) Daily run-off averaged over the whole catchment area over the 2000–2018 period.

The catchment hydrology understanding, at Parlung No. 4 and elsewhere, will be improved in the future by utilizing a more physically based, land-surface model which incorporates detailed parameterizations of phase change thresholds [22] and account for meltwater refreezing [33] as well as surface and wind-driven sublimation [34].

4.2.2. Conclusions

Our research has shown that a combination of field observations, remote sensing and modeling is crucial to unravel the response of High Mountain Asia catchments to climate. Remote sensing datasets on albedo, snow cover and geodetic mass balance have been vital to correctly calibrate and constrain the model that we used in WP5 to understand the contributions of snow, ice melt and precipitation to runoff, and reconstruct their variability in space and time. We have quantified, for the first time, key aspects of debris-covered glacier processes, including debris actual distribution, the importance of cliffs and ponds for glacier mass balance, and their evolution in time. We have shown that debris-covered glaciers have a distinct response to climate in comparison to clean ice glaciers, and in particular that the changes induced by the monsoon combine with debris-covered ice to reduce melt rates during the main melting season.

Our overall work, spanning field research, methodological developments of products from remote sensing data, and modeling has also pointed out to two clear needs: (1) the need to setup and investigate a large number of benchmark catchments where processes can be studied in a systematic manner to allow comparison of the distinct response of catchments with different glacier and climate characteristics; (2) the need for models of a new generation that includes a physically based representation of processes.

4.3. Forcing, Calibration, Validation and Data Assimilation in Basin Scale Hydrological Models Using Satellite Data Products

4.3.1. Results

(1) Establishment of a watershed observing system

During the HiWATER experiment [35], an integrated observatory network was established in the Heihe River Basin [16]. The network consists of a hydrometeorological observatory, a wireless sensor network, synchronized ground measurements and satellite remote sensing observatory network. All the datasets of the network have been publicly released under an open data protocol [36,37], which would benefit the scientific community of earth and environmental science and many other disciplines.

(2) Development of a watershed system model

We developed a watershed system model (see Figure 10) by coupling ecohydrological and socioeconomic systems [38]. The model is mainly composed of an integrated ecohydrological model developed by loosely coupling the geomorphology-based ecohydrological model with the hydrological–ecological integrated watershed-scale flow (HEIFLOW) model [14,39,40], a socioeconomic model [41], and two interface models. The watershed system model proved to be reliable in simulating multiple eco-hydrological processes and

showed good skills in closing the water balance at multiple spatial scales [38]. This integrated modeling system supports a better understanding of the eco-hydrological responses to water management measures, and the development of the scientifically based decision support system. The model could advance our understanding of the water-land-air-plant-human nexus at the watershed scale.

We systematically estimated the water balance of HRB from 2001 to 2012 using this watershed system model. As shown in Figure 10 [38], the key elements of the hydrological cycle are quantified. Specifically, the mean annual precipitation was approximately 589.5 mm a^{-1} in the upstream basin, with 407.1 mm being rain and 182.4 mm snow. Annual water loss due to ET was approximately 376.5 mm a^{-1}, most of which at elevations below 4500 m, i.e., at higher temperature. The annual streamflow was about 3.04 × 10^9 m^3 a^{-1}. The rapid glacial retreat resulted in a negative change in glacier water storage, and an increasing trend was observed in groundwater and soil water storage, which might be attributed to the increase in precipitation.

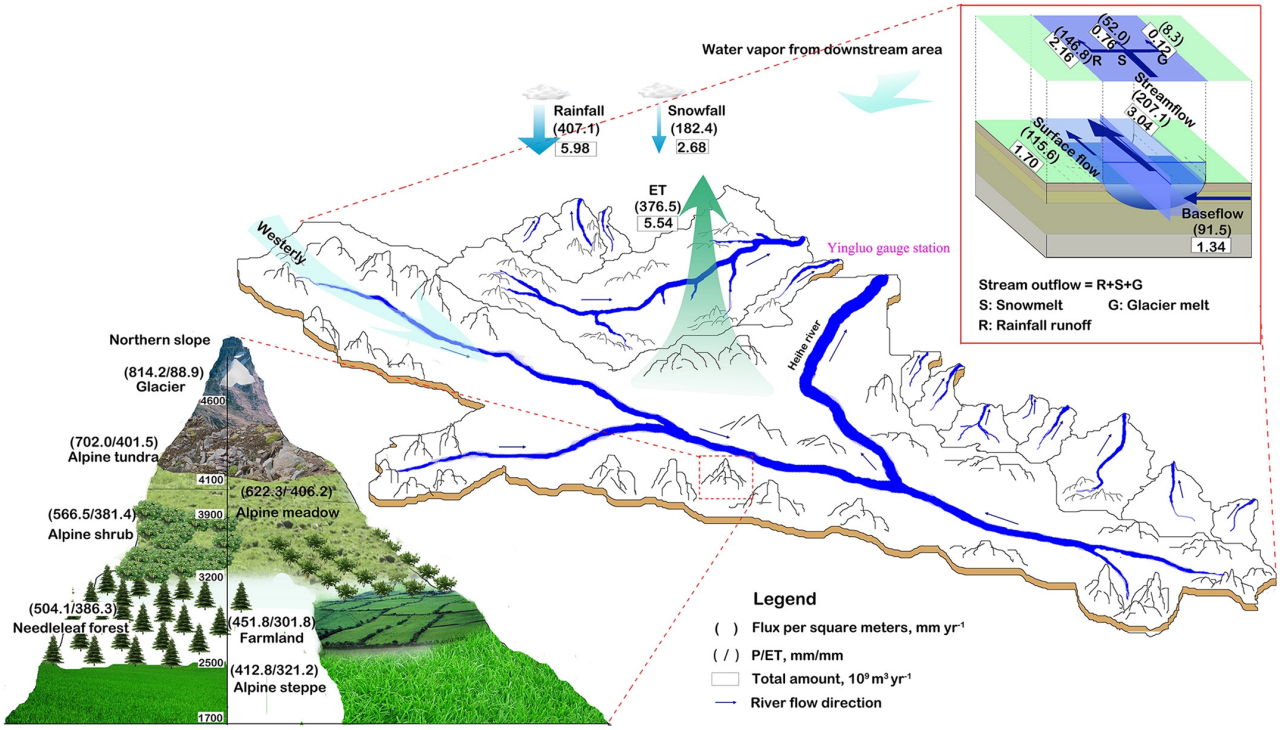

Figure 10. Hydrological cycle in the upstream area of the Heihe River Basin based on the proposed watershed system model, according to Li et al. [38].

The long-term (2001–2060) trends in streamflow and water storage were evaluated by applying this modeling system. As shown in Figure 11 [42], significant variations in stream flow were obtained in three hydrological stations, Yingluo Gorge, Zhengyi Gorge and Langxinshan. All the stations witnessed an increasing trend in 2001–2016 against a downward trend in 2017–2060, This finding may suggest a conflict in water-use between humans and ecosystems in the future. Interventions in the water management system should be put in place to ensure sustainable and shared use of water resources among agriculture, groundwater, and ecosystems prior to the occurrence of such conflict.

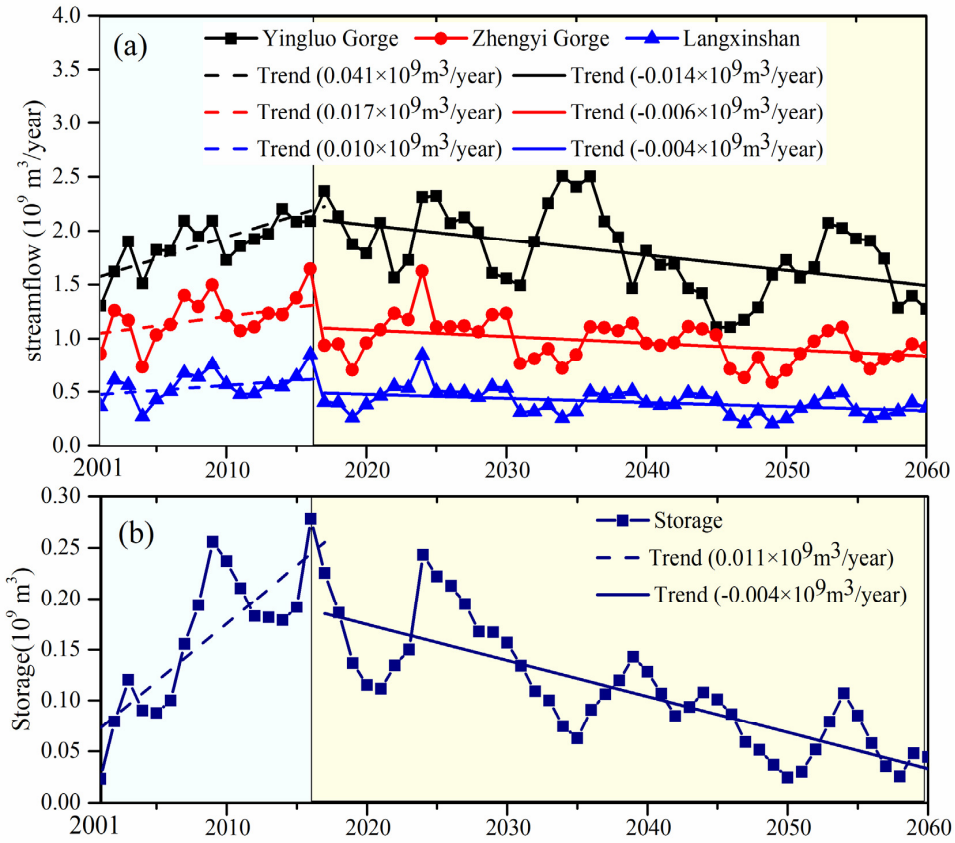

Figure 11. Long-term streamflow simulations (**a**) at the Yingluo Gorge, Zhengyi Gorge and Langxinshan stations, and water storage simulations (**b**) of the terminal lake (Sogo Nuur) within the HRB from Li et al. [42].

(3) Implementation of a multivariate land data assimilation system

An updated and parallelized data assimilation system scheme was implemented. A soil moisture assimilation scheme that jointly assimilates the brightness temperature of Advanced Microwave Scanning Radiometer (AMSR)–Earth Observing System and Land Surface Temperature products retrieved with the data acquired by the MODIS was developed [43]. This system corrects correct model bias by simultaneously updating model states and parameters with a dual ensemble Kalman filter. The results show that the soil moisture retrievals were improved by assimilating AMSR-E Brightness Temperature and MODIS LST (Figure 12). In addition, we developed a physically based hydrological data assimilation system using the gridded and parallelized SWAT distributed hydrological model [44]. The system integrates remotely sensed and ground-based observations by applying a Parallel Data Assimilation Framework. The system could accurately characterize watershed hydrological states and fluxes. As to the application of data assimilation to hydrological water flows, significant progress has been achieved as well. For instance, Pan et al. [45] assimilated two satellite precipitation products, i.e., retrieved with the data acquired by the TRMM and FY-2D, into the WRF model applying the 4D-Var data assimilation method in Heihe River Basin. An improved precipitation forecasting has been observed. Besides, a nonlinear and non-Gaussian land data assimilation platform has been implemented, which integrated multiple model operators, observation operators and non-linear data assimilation algorithms [42,46].

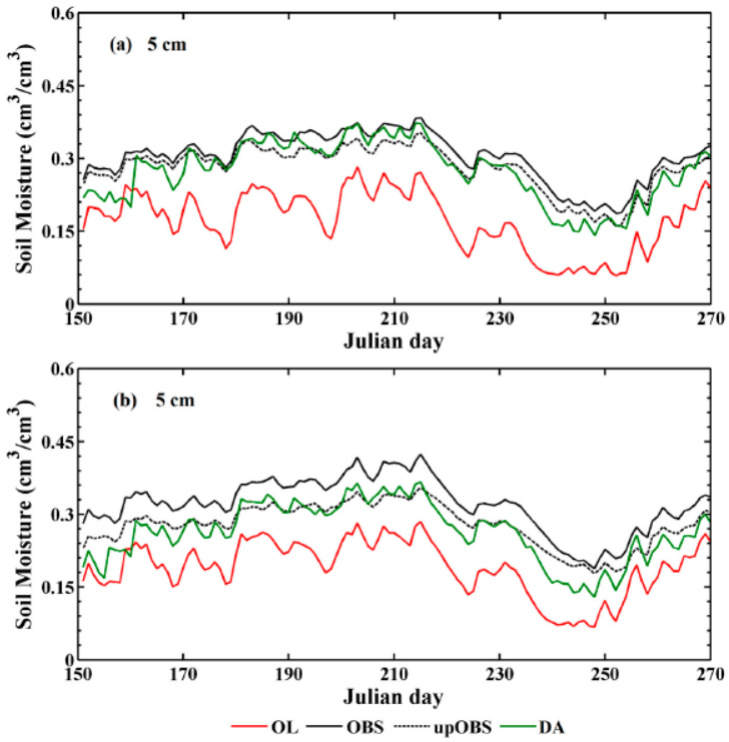

Figure 12. Daily surface soil moisture derived from simulation and assimilation with the average measurements and upscaled measurements in the: medium grid (**a**) and large grid (**b**) according to Chen et al. [43].

The FEST-EWB model has been calibrated and validated in two case studies: the Chiese Irrigation Consortium in Northern Italy and the Heihe basin in China. In the Chiese basin, the FEST-EWB model was run at the temporal resolution of 1 h and at the spatial resolution of 250 m. The years from 2005 to 2010 were used for calibration while the years from 2011 to 2016 for model validation. In the Heihe basin FEST-EWB was run at 1 km spatial resolution for the year 2012 at hourly scale.

Satellite LST data were used to calibrate the soil parameters of FEST-EWB model in both river basins. The Chiese calibration with the original parameters gave a mean absolute pixel-wise underestimation of satellite LST by 5.2 °C, while after the calibration, this was reduced to 3.4 °C. Smaller differences between satellite and simulated LST, i.e., about 2 °C, were obtained after calibration especially in the southernmost area of the basin, i.e., the alluvial plain with widespread irrigation. Calibration also helps improving the model performance in the mountainous northernmost area. The calibration and validation results have been described in detail by Paciolla et al. [47] for the Heihe case study and Corbari and Mancini [9] for the Chiese Irrigation Consortium.

The FEST-EWB results have been validated at local scales (Table 3) by comparing the observed and simulated latent (LE) and sensible (H) heat fluxes and SSM at the eddy covariance station installed in the same maize field in 2016, 2017 and 2018 for the Chiese area and at Daman and Yingke stations in the Heihe basin irrigated area. The validation statistics are detailed in Table 3, in terms of Root Mean Square Error (RMSE), slope of the linear interpolation (m) and determination coefficient (R^2).

The FEST-EWB estimates of evaporation and transpiration (ET) in the Heihe basin were compared with five satellite data products on ET: high resolution ETMonitor [44], ERA-Interim [48], GLDAS2 [49], GLEAM [50] and MERRA2 [51]. The scatter plots (Figure 13) show that ET from ET Monitor and FEST-EWB are in good agreement with the higher spatial resolution model estimates, after the calibration for this case study. Regarding the global datasets, ERAInterim is the only data product able to roughly follow the FEST-

EWB estimates, despite the large difference in spatial resolution. GLDAS2, GLEAM and MERRA2 are considerably underestimating ET compared with FEST-EWB and ETMonitor.

Table 3. FEST-EWB validation against eddy covariance measurements of latent (LE) and sensible (H) heat flux at two locations in the Heihe and one location in the Chiese river basins.

Heihe River Basin					Chiese River Basin				
Station	**Evaluated Item**	**RMSE**	**m**	**R^2**	**Year**	**Evaluated Item**	**RMSE**	**m**	**R^2**
Daman	LE	47	0.44	0.63	2016	SSM	0.03	0.89	0.75
	H	48	0.76	0.53		LE	25.7	0.94	0.8
						H	38.3	0.99	0.79
Yingke	LE	44	0.5	0.66	2017	SSM	0.1	0.78	0.65
	H	49	0.73	0.54		LE	49	0.93	0.7
						H	78	1.1	0.8
					2018	SSM	0.07	0.8	0.7
						LE	43	1.1	0.67
						H	50	1.2	0.83

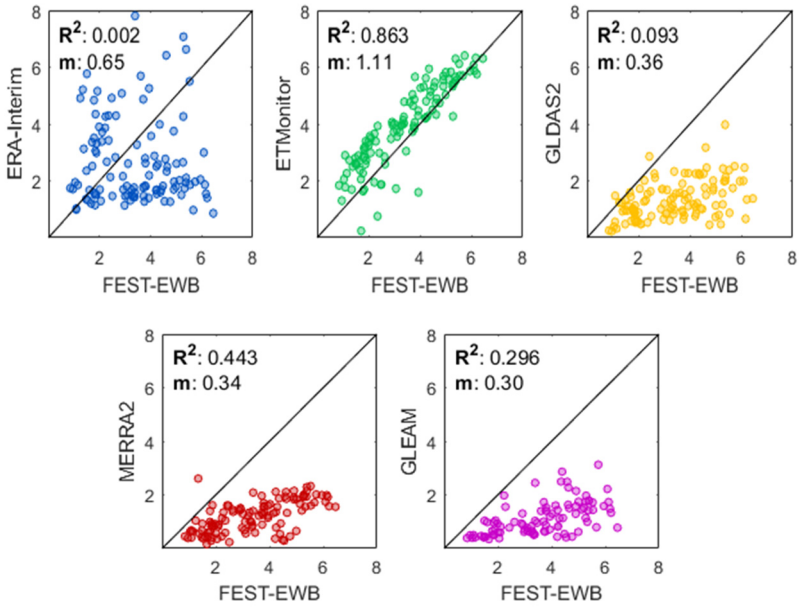

Figure 13. Comparison of the different ET products (in mm/day) over the Heihe basin for one year of simulation.

4.3.2. Conclusions

Data assimilation of the microwave brightness temperature and of the land surface temperature clearly improved model estimates of surface soil moisture. Likewise, assimilation of precipitation data products is an advanced land–atmosphere model significantly improved precipitation forecasts. Use of data assimilation to improve estimates of model parameters was demonstrated by a pilot study in Italy. Initial estimates of soil properties were improved by assimilating retrievals of land surface temperature.

The ecohydrological research over HRB in terms of the hydrological observation, modeling and data assimilation has been witnessed huge progress. The Chinese Academy of Sciences is performing the Second Tibetan Plateau Scientific Expedition (STEP) Program. The Qilian mountain and other endorheic river basins are the key expedition regions. The scientific findings and practical experiences of HRB should and could provide useful prior knowledge for the program. Simultaneously, the observing system design scheme, modeling idea and data assimilation systems can be extensively examined, extended and widely applied in a more generic context and to larger river basins.

4.4. Monitoring Water Resources in Red River Basin Using Microwave Remote Sensing

4.4.1. Results

Soil moisture products from the SMAP mission were used in this study: the Enhanced Level 3 Radiometer Global Daily 9 km EASE-Grid Soil Moisture. SMAP SSM products were used as an input to a disaggregation algorithm, DISPATCH (DISaggregation based on a Physical and Theoretical scale Change; Merlin et al. [52]), in order to obtain near surface soil moisture at 1 km resolution. DISPATCH disaggregates low-resolution SSM to 1 km SSM by using a soil evaporative efficiency (SEE) metric at 1 km to model the spatial variability within a low-resolution pixel. SEE, defined as the ratio of actual to potential evaporation, is derived using Land Surface Temperature (LST) and Normalized Difference Vegetation Index (NDVI) data from MODIS. The distribution of the high-resolution SSM around the mean value of the low-resolution SSM products is determined by the spatial link between the optical-derived SEE and SSM [53]. A more detailed description of the disaggregation methodology can be found in Merlin et al. [52].

Figure 14 shows the temporal evolution of soil moisture at high spatial resolution. The plot clearly depicts the seasonal evolution with higher soil moisture values during July–August corresponding to the wet season. The 1 km SSM was compared to the measurements obtained during the Soil Moisture Experiment in the Luan River (SMELR) from 2017 to 2018 in the semi-arid Luan River watershed located in the North of China [54].

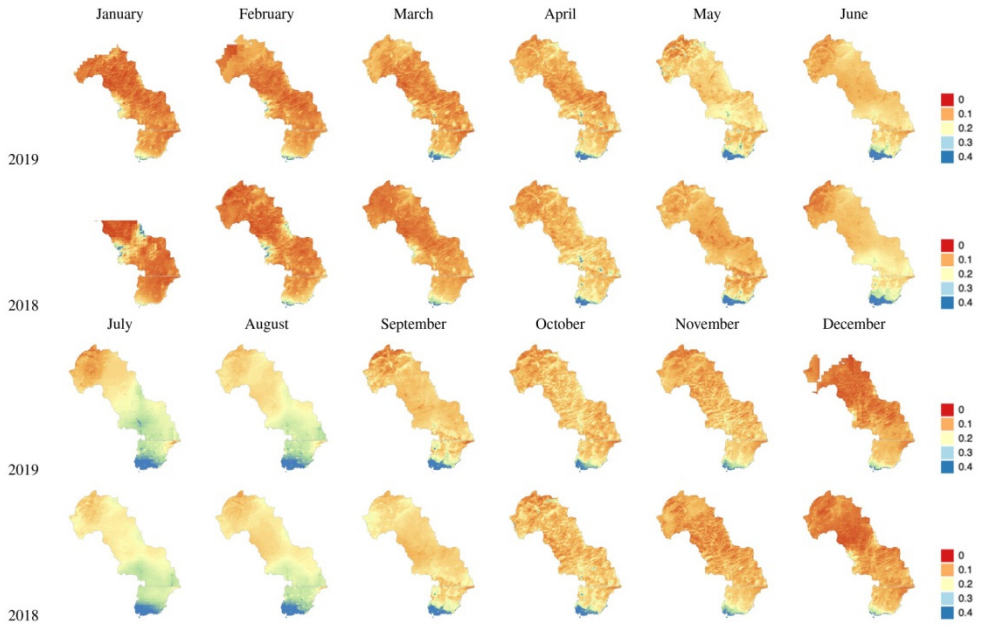

Figure 14. Monthly soil moisture in the Luan River basin.

The comparison of the Soil Moisture Products is shown in Figure 15. The figure shows that most of the stations gave a good value of correlation and low values of RMSE and bias (except in two stations).

Water level was estimated both from Sentinel-3 Level-2 and Level-1B as in Gao et al. [55]. When using Level-1B data, two retrackers (namely the Offset Center of Gravity (OCOG) retracker and two-step SAR physical-based retracker), together with a waveform portion selection method, were used to minimize land contamination in the waveforms and to select the nadir return associated with the water body being overflown. The waveform portion selection method, with consideration of the DEM, was used to fit the multi-peak waveforms that arise when overflying the continental water bodies, exploiting a sub-waveform-based approach to pick up the one corresponding to the nadir.

SWAT model requires several meteorological forcing variables. We calculated daily maximum temperature, minimum temperature, precipitation, relative humidity and short-

wave solar radiation and average wind speed based on GLDAS_NOAH025_3H dataset. We employed two alternative microwave precipitation products and three microwave satellite precipitation products: CMORPH and gauges merged 0.1° precipitation dataset (MNIC), IMERG-Early and TMPA-RT. In the previous runoff simulation, the comparisons among TMPA-RT, IMERG-Early, MNIC and GLDAS precipitation datasets in 2018, MNIC, TMPA-RT and IMERG-Early showed better performances as in Li et al. [42]. Then, we estimated water level at Yuanjiang station based on discharge rating curve and further compared model estimates with water level retrieved by SAR altimetry.

Figure 16c shows water level at a virtual station called 289_S3B estimated from four different retrackers. This virtual station is the closest to the hydrological station named Yuangjan (Figure 16b). Unfortunately, water levels from simulations (Figure 16a) and water level from S3B have different timelines as a consequence from S3 changes on the DEM; therefore, we can only retrieve correct water levels starting on 2020.

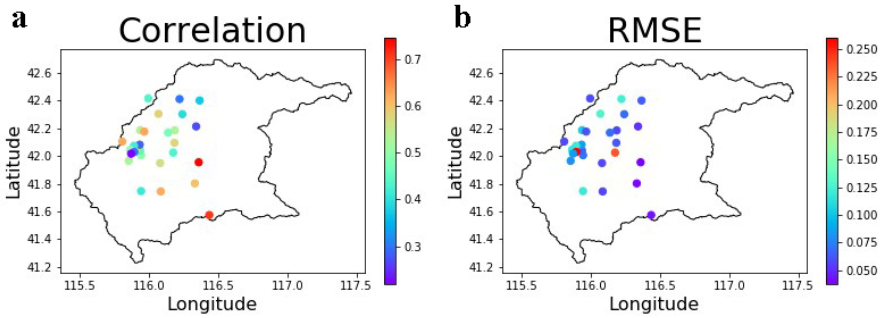

Figure 15. Retrievals of Soil Moisture vs. in-situ soil moisture measurements at stations from the SMELR [54] experiment: (**a**) Correlation and (**b**) RSME.

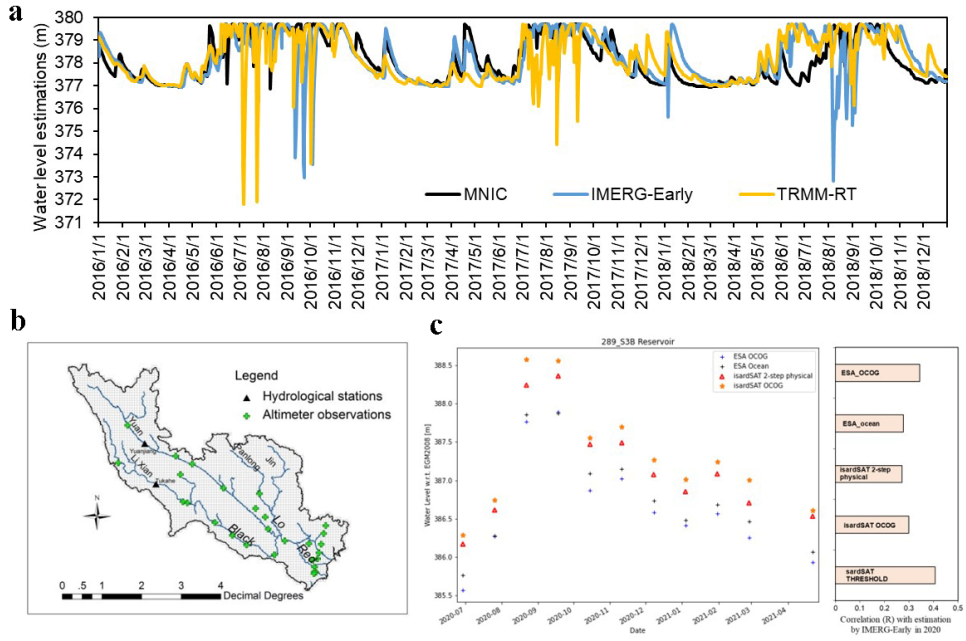

Figure 16. Observations on the terrestrial water cycle in the Red River: (**a**) comparison of water level estimations from MNIC, IMERG-Early and TRMM-RT precipitation datasets based on SWAT model in the upstream of the Red River Basin; (**b**) locations of S3 Altimeter (SRAL) observations. (**c**) S3/SRAL: comparison of the water level of the Red River retrieved with the L2 OCOG and Ocean retrackers and with L1B using isardSAT's own retrackers and their correlation efficient (R) with water level estimations by IMERG-Early in 2020.

4.4.2. Conclusions

The results summarized above lead to two general conclusions:

(a) A higher spatial resolution of data products on SSM is necessary for studies on specific river basins. Different solutions have been proposed in literature to downscale SSM data, including the one documented in this study;

(b) The Red River case study has demonstrated that usable measurements of water level can be retrieved from the S3/RA data even from water targets smaller than the satellite footprint. This requires advanced data processing as described.

The limited case study on hydrologic modeling with SWAT showed that there is potential for model calibration and validation using measurements of water level by S3/RA.

5. Main Conclusions

The results summarized above clearly document the path toward full integration of satellite retrievals with modeling of cryospheric and hydrologic processes to link the terrestrial water cycle at high elevation with multiple forms of water use at lower elevation. New data products have been generated, such as glacier surface flow velocity and glacier mass balance, and previous capabilities, such as the ones of the ETMonitor system, have been extended to estimate sublimation of snow and ice. The latter, in combination with improvements in the retrievals of ice and snow albedo, feed directly into the development of detailed models of glacier energy and mass balance models.

The improved retrieval of snow and ice albedo is particularly important in this context since albedo is the main driver of the response of snow and ice mass balance to weather variability. The improved retrieval method has been applied to study the evolution of glacier albedo in the WNM in 2000–2019, documenting the overall trend, the interannual and seasonal variability. The glacier albedo at high spatial resolution is a key input to the two models of glacier energy and mass balance described above. This is particularly relevant when the glacier surface is rather heterogeneous with fresh snow, clean ice, surface deposits of fine particles and debris. Other forcing variables, e.g., air temperature, should also be mapped at the same spatial resolution, but it remains a challenge, although alternate solutions have been explored. Likewise, hillslope hydrology, experimental and modeling studies on the terrestrial water cycle at high elevation require well-equipped reference catchments.

We have carried out multiple studies on modeling of entire watersheds, i.e., linking the generation of fresh water through snow and ice melting with water uses. Taken together, these studies clearly show the value of model calibration and validation using satellite retrievals on the terrestrial water cycle. Three different data assimilation approaches have been successfully applied to model two river basins. In one case, an integrated watershed model was applied to evaluate the response of water flows to a scenario on climate variability in the period 2001–2060. In such studies, data-assimilation is beneficial if applied to the estimation of model parameters.

Our research has shown that a combination of field observations, remote sensing and modeling is crucial to unravel the response of High Mountain Asia catchments to climate.

The system can now generate time series of data products on snow and ice sublimation across a range of spatial resolutions. Studies on the observation of glacier were rather comprehensive and focused particularly on glacier albedo, which controls radiative forcing of glacier mass balance and the coupling of the cryosphere with the atmosphere.

We have shown that debris-covered glaciers have a distinct response to climate in comparison to clean ice glaciers, and in particular that the changes induced by the monsoon combine with debris-covered ice to reduce melt rates during the main melting season.

The scientific findings and practical experiences of HRB should and could provide useful prior knowledge for the program. Simultaneously, the observing system design scheme, modeling idea and data assimilation systems can be extensively examined, extended and widely applied in a more generic context and to larger river basins.

Author Contributions: Conceptualization, M.M. (Massimo Menenti), X.L., L.J., K.Y., F.P., M.M. (Marco Mancini), J.S., M.J.E., Q.L., Y.Q. and C.C.; methodology, M.J.E., C.H., J.Z. (Ji Zhou), X.H., X.P., H.L., C.Z., Q.C., J.L., J.Z. (Jie Zhou), G.H., Y.W., B.D., W.Y., P.B., M.J.M., E.S.M., T.E.S., C.M., Y.Z., R.L., T.Z., V.S., Q.G., J.Z. (Jingxiao Zhang), S.R., Q.X., N.W., Y.S., X.M., J.Z. (Jing Zhang), J.J., A.P.J., M.K., S.F., N.P. and G.P.; validation. V.S. and G.P.; formal analysis, C.C., J.Z. (Jingxiao Zhang), S.R., Q.X., N.W., Y.S., X.M., J.Z. (Jing Zhang), J.J., A.P.J., M.K., S.F., N.P. and G.P.; resources, M.M. (Massimo Menenti), X.L., L.J., K.Y., F.P. and T.Z.; writing—original draft preparation, M.M. (Massimo Menenti); writing—review and editing, X.L., L.J., K.Y., F.P., M.M. (Marco Mancini), J.S., M.J.E. and S.R.; supervision, M.M. (Massimo Menenti); project administration, M.M. (Massimo Menenti), X.L., L.J., K.Y., F.P., M.M. (Marco Mancini), J.S. and M.J.E.; funding acquisition, M.M. (Massimo Menenti), X.L., L.J., K.Y., F.P., M.M. (Marco Mancini), J.S. and M.J.E. All authors have read and agreed to the published version of the manuscript.

Funding: The work was supported by the Strategic Priority Research Program of Chinese Academy of Sciences (Grant No. XDA19070102, XDA19030203 and XDA20100309), the National Natural Science Foundation of China (Grant No. 91737205, 42071404 and 41671355), the Second Tibetan Plateau Scientific Expedition and Research Program (STEP) (Grant No. 2019QZKK0103), the Chinese Academy of Sciences President's Inter-national Fellowship Initiative (Grant No. 2020VTA0001), the MOST High Level Foreign Expert Program (Grant No. GL20200161002) and the ESA Dragon 4 YSS Program (Grant No. 4000121196).

Data Availability Statement: Data are available under well-established policies within the Dragon Program.

Conflicts of Interest: The authors declare no conflict of interest.

References

1. Beniston, M.; Farinotti, D.; Stoffel, M.; Andreassen, L.M.; Coppola, E.; Eckert, N.; Fantini, A.; Giacona, F.; Hauck, C.; Huss, M.; et al. The European mountain cryosphere: A review of its current state, trends, and future challenges. *Cryosphere* **2018**, *12*, 759–794. [CrossRef]
2. Menenti, M.; Su, B.; de Michele, C.; Jia, L.; Sobrino, J.; Ma, Y.; Yan, Y.; Li, X.; Ueno, K.; Bastiaansen, W.; et al. *Coordinated Asia–European Long-Term Observing System of Qinghai—Tibet Plateau Hydro-Meteorological Processes and the Asian-Monsoon System with Ground Satellite Image Data and Numerical Simulations (CEOP-AEGIS). Final Report*; University of Strasbourg: Strasbourg, France, 2014; ISSN 2118-7843.
3. Barnett, T.P.; Dümenil, L.; Schlese, U.; Roeckner, E. The Effect of Eurasian Snow Cover on Global Climate. *Science* **1988**, *239*, 504–507. [CrossRef] [PubMed]
4. Mastrotheodoros, T.; Pappas, C.; Molnar, P.; Burlando, P.; Manoli, G.; Parajka, J.; Rigon, R.; Szeles, B.; Bottazzi, M.; Hadjidoukas, P.; et al. More green and less blue water in the Alps during warmer summers. *Nat. Clim. Chang.* **2020**, *10*, 155–161. [CrossRef]
5. Wood, E.F.; Roundy, J.K.; Troy, T.J.; van Beek, R.; Bierkens, M.; Blyth, E.; de Roo, A.; Döll, P.; Ek, M.; Famiglietti, J.; et al. Reply to comment by Keith, J. Beven and Hannah, L. Cloke on "hyperresolution global land surface modeling: Meeting a grand challenge for monitoring Earth's terrestrial water". *Water Resour. Res.* **2012**, *48*. [CrossRef]
6. Zhong, B.; Yang, A.; Nie, A.; Yao, Y.; Zhang, H.; Wu, S.; Liu, Q. Finer Resolution Land-Cover Mapping Using Multiple Classifiers and Multisource Remotely Sensed Data in the Heihe River Basin. *IEEE J. Sel. Top. Appl. Earth Obs. Remote. Sens.* **2015**, *8*, 4973–4992. [CrossRef]
7. Wang, T.; Zhang, G.; Li, D.; Tang, X.; Jiang, Y.-H.; Pan, H.-B.; Zhu, X.; Fang, C. Geometric Accuracy Validation for ZY-3 Satellite Imagery. *IEEE Geosci. Remote. Sens. Lett.* **2014**, *11*, 1168–1171. [CrossRef]
8. Pan, X.; Tian, X.; Li, X.; Xie, Z.; Shao, A.; Lu, C. Assimilating Doppler radar radial velocity and reflectivity observations in the weather research and forecasting model by a proper orthogonal-decomposition-based ensemble, three-dimensional variational assimilation method. *J. Geophys. Res. Space Phys.* **2012**, *117*. [CrossRef]
9. Corbari, C.; Ravazzani, G.; Mancini, M. A distributed thermodynamic model for energy and mass balance computation: FEST-EWB. *Hydrol. Process.* **2010**, *25*, 1443–1452. [CrossRef]
10. Ravazzani, G.; Mancini, M.; Giudici, I.; Amadio, P. Effects of soil moisture parameterization on a real-time flood forecasting system based on rainfall thresholds. *Proc. IAHS-AISH Publ.* **2007**, *313*, 4017.
11. Corbari, C.; Mancini, M. Calibration and Validation of a Distributed Energy–Water Balance Model Using Satellite Data of Land Surface Temperature and Ground Discharge Measurements. *J. Hydrometeorol.* **2014**, *15*, 376–392. [CrossRef]
12. Corbari, C.; Ravazzani, G.; Martinelli, J.; Mancini, M. Elevation based correction of snow coverage retrieved from satellite images to improve model calibration. *Hydrol. Earth Syst. Sci.* **2009**, *13*, 639–649. [CrossRef]
13. Chen, Q.; Jia, L.; Menenti, M.; Hutjes, R.; Hu, G.; Zheng, C.; Wang, K. A numerical analysis of aggregation error in evapotranspiration estimates due to heterogeneity of soil moisture and leaf area index. *Agric. For. Meteorol.* **2019**, *269–270*, 335–350. [CrossRef]

14. Zheng, C.; Jia, L. Global canopy rainfall interception loss derived from satellite earth observations. *Ecohydrology* **2020**, *13*, e2186. [CrossRef]
15. Wang, N.; Jia, L.; Zheng, C.; Menenti, M. Estimation of subpixel snow sublimation from multispectral satellite observations. *J. Appl. Remote Sens.* **2017**, *11*, 046017. [CrossRef]
16. Liu, S.; Li, X.; Xu, Z.; Che, T.; Xiao, Q.; Ma, M.; Liu, Q.; Jin, R.; Guo, J.; Wang, L.; et al. The Heihe Integrated Observatory Network: A Basin-Scale Land Surface Processes Observatory in China. *Vadose Zone J.* **2018**, *17*, 1–21. [CrossRef]
17. Ma, Y.; Hu, Z.; Xie, Z.; Ma, W.; Wang, B.; Chen, X.; Li, M.; Zhong, L.; Sun, F.; Gu, L.; et al. A long-term (2005–2016) dataset of hourly integrated land–atmosphere interaction observations on the Tibetan Plateau. *Earth Syst. Sci. Data* **2020**, *12*, 2937–2957. [CrossRef]
18. Jia, L.; Zheng, C.; Hu, G.C.; Menenti, M. 4.03—Evapotranspiration. In *Comprehensive Remote Sensing*; Liang, S., Ed.; Elsevier: Oxford, UK, 2018; pp. 25–50. ISBN 9780128032213.
19. Ren, S.; Menenti, M.; Jia, L.; Zhang, J.; Zhang, J.; Li, X. Glacier Mass Balance in the Nyainqentanglha Mountains between 2000 and 2017 Retrieved from ZiYuan-3 Stereo Images and the SRTM DEM. *Remote Sens.* **2020**, *12*, 864. [CrossRef]
20. Zhang, J.; Jia, L.; Menenti, M.; Ren, S. Interannual and Seasonal Variability of Glacier Surface Velocity in the Parlung Zangbo Basin, Tibetan Plateau. *Remote Sens.* **2020**, *13*, 80. [CrossRef]
21. Ren, S.; Miles, E.S.; Jia, L.; Menenti, M.; Kneib, M.; Buri, P.; McCarthy, M.J.; Shaw, T.E.; Yang, W.; Pellicciotti, F. Anisotropy parameterization development and evaluation for glacier surface albedo retrieval from satellite observations. *Remote Sens.* **2021**, *13*, 1714. [CrossRef]
22. Ding, B.; Yang, K.; Yang, W.; He, X.; Chen, Y.; Lazhu; Guo, X.; Wang, L.; Wu, H.; Yao, T. Development of a Water and Enthalpy Budget-based Glacier mass balance Model (WEB-GM) and its preliminary validation. *Water Resour. Res.* **2017**, *53*, 3146–3178. [CrossRef]
23. Shaw, T.E.; Yang, W.; Ayala, Á.; Bravo, C.; Zhao, C.; Pellicciotti, F. Distributed summer air temperatures across mountain glaciers in the south-east Tibetan Plateau: Temperature sensitivity and comparison with existing glacier datasets. *Cryosphere* **2021**, *15*, 595–614. [CrossRef]
24. Girona-Mata, M.; Miles, E.S.; Ragettli, S.; Pellicciotti, F. High-Resolution Snowline Delineation From Landsat Imagery to Infer Snow Cover Controls in a Himalayan Catchment. *Water Resour. Res.* **2019**, *55*, 6754–6772. [CrossRef]
25. Herreid, S.; Pellicciotti, F. The state of rock debris covering Earth's glaciers. *Nat. Geosci.* **2020**, *13*, 621–627. [CrossRef]
26. Kneib, M.; Miles, E.; Jola, S.; Buri, P.; Herreid, S.; Bhattacharya, A.; Watson, C.; Bolch, T.; Quincey, D.; Pellicciotti, F. Mapping ice cliffs on debris-covered glaciers using multispectral satellite images. *Remote Sens. Environ.* **2021**, *253*, 112201. [CrossRef]
27. Miles, E.S.; Willis, I.C.; Arnold, N.S.; Steiner, J.; Pellicciotti, F. Spatial, seasonal and interannual variability of supraglacial ponds in the Langtang Valley of Nepal, 1999–2013. *J. Glaciol.* **2017**, *63*, 88–105. [CrossRef]
28. Herreid, S.; Pellicciotti, F. Automated detection of ice cliffs within supraglacial debris cover. *Cryosphere* **2018**, *12*, 1811–1829. [CrossRef]
29. Steiner, J.F.; Buri, P.; Miles, E.S.; Ragettli, S.; Pellicciotti, F. Supraglacial ice cliffs and ponds on debris-covered glaciers: Spatio-temporal distribution and characteristics. *J. Glaciol.* **2019**, *65*, 617–632. [CrossRef]
30. Buri, P.; Pellicciotti, F. Aspect controls the survival of ice cliffs on debris-covered glaciers. *Proc. Natl. Acad. Sci. USA* **2018**, *115*, 4369–4374. [CrossRef] [PubMed]
31. Buri, P.; Miles, E.S.; Steiner, J.F.; Ragettli, S.; Pellicciotti, F. Supraglacial Ice Cliffs Can Substantially Increase the Mass Loss of Debris-Covered Glaciers. *Geophys. Res. Lett.* **2021**, *48*, e2020GL092150. [CrossRef]
32. Miles, E.S.; Willis, I.; Buri, P.; Steiner, J.F.; Arnold, N.S.; Pellicciotti, F. Surface Pond Energy Absorption Across Four Himalayan Glaciers Accounts for 1/8 of Total Catchment Ice Loss. *Geophys. Res. Lett.* **2018**, *45*, 10–464. [CrossRef] [PubMed]
33. Stigter, E.E.; Steiner, J.F.; Koch, I.; Saloranta, T.M.; Kirkham, J.D.; Immerzeel, W.W. Energy and mass balance dynamics of the seasonal snowpack at two high-altitude sites in the Himalaya. *Cold Reg. Sci. Technol.* **2021**, *183*, 103233. [CrossRef]
34. Ayala, A.; Pellicciotti, F.; MacDonell, S.; McPhee, J.; Burlando, P. Patterns of glacier ablation across North-Central Chile: Identifying the limits of empirical melt models under sublimation-favorable conditions. *Water Resour. Res.* **2017**, *53*, 5601–5625. [CrossRef]
35. Li, X.; Cheng, G.; Lin, H.; Cai, X.; Fang, M.; Ge, Y.; Yingchun, G.; Chen, M.; Li, W. Watershed System Model: The Essentials to Model Complex Human-Nature System at the River Basin Scale. *J. Geophys. Res. Atmos.* **2018**, *123*, 3019–3034. [CrossRef]
36. Li, X.; Cheng, G.; Liu, S.; Xiao, Q.; Ma, M.; Jin, R.; Che, T.; Liu, Q.; Wang, W.; Qi, Y.; et al. Heihe watershed allied telemetry experimental research (HiWater) scientific objectives and experimental design. *Bull. Am. Meteorol. Soc.* **2013**, *94*, 1145–1160. [CrossRef]
37. Che, T.; Li, X.; Liu, S.; Li, H.; Xu, Z.; Tan, J.; Zhang, Y.; Ren, Z.; Xiao, L.; Deng, J.; et al. Integrated hydrometeorological, snow and frozen-ground observations in the alpine region of the Heihe River Basin, China. *Earth Syst. Sci. Data* **2019**, *11*, 1483–1499. [CrossRef]
38. Li, X.; Liu, S.; Xiao, Q.; Ma, M.; Jin, R.; Che, T.; Wang, W.; Hu, X.; Xu, Z.; Wen, J.; et al. A multiscale dataset for understanding complex eco-hydrological processes in a heterogeneous oasis system. *Sci. Data* **2017**, *4*, 170083. [CrossRef]
39. Li, X.; Zhang, L.; Zheng, Y.; Yang, D.; Wu, F.; Tian, Y.; Han, F.; Gao, B.; Li, H.; Zhang, Y.; et al. Novel hybrid coupling of ecohydrology and socioeconomy at river basin scale: A watershed system model for the Heihe River basin. *Environ. Model. Softw.* **2021**, *141*, 105058. [CrossRef]

40. Tian, Y.; Zheng, Y.; Han, F.; Zheng, C.; Li, X. A comprehensive graphical modeling platform designed for integrated hydrological simulation. *Environ. Model. Softw.* **2018**, *108*, 154–173. [CrossRef]
41. Han, F.; Zheng, Y.; Tian, Y.; Li, X.; Zheng, C. Accounting for field-scale heterogeneity in the ecohydrological modeling of large arid river basins: Strategies and relevance. *J. Hydrol.* **2021**, *595*, 126045. [CrossRef]
42. Wu, F.; Bai, Y.; Zhang, Y.; Li, Z. Balancing water demand for the Heihe River Basin in Northwest China. *Phys. Chem. Earth* **2017**, *101*, 178–184. [CrossRef]
43. Chen, W.; Shen, H.; Huang, C.; Li, X. Improving Soil Moisture Estimation with a Dual Ensemble Kalman Smoother by Jointly Assimilating AMSR-E Brightness Temperature and MODIS LST. *Remote Sens.* **2017**, *9*, 273. [CrossRef]
44. Zhang, Y.; Cheng, G.; Li, X.; Jin, H.; Yang, D.; Flerchinger, G.N.; Chang, X.; Bense, V.F.; Han, X.; Liang, J. Influences of Frozen Ground and Climate Change on Hydrological Processes in an Alpine Watershed: A Case Study in the Upstream Area of the Hei'he River, Northwest China. *Permafr. Periglac. Process.* **2017**, *28*, 420–432. [CrossRef]
45. Pan, X.; Li, X.; Cheng, G.; Hong, Y. Effects of 4D-Var Data Assimilation Using Remote Sensing Precipitation Products in a WRF Model over the Complex Terrain of an Arid Region River Basin. *Remote Sens.* **2017**, *9*, 963. [CrossRef]
46. Liu, F.; Wang, L.; Li, X.; Huang, C. ComDA: A common software for nonlinear and Non-Gaussian Land Data Assimilation. *Environ. Model. Softw.* **2020**, *127*, 104638. [CrossRef]
47. Paciolla, N.; Corbari, C.; Hu, G.; Zheng, C.; Menenti, M.; Jia, L.; Mancini, M. Evapotranspiration estimates from an energy-water-balance model calibrated on satellite land surface temperature over the Heihe basin. *J. Arid. Environ.* **2021**, *188*, 104466. [CrossRef]
48. Dee, D.P.; Uppala, S.M.; Simmons, A.J.; Berrisford, P.; Poli, P.; Kobayashi, S.; Andrae, U.; Balmaseda, M.A.; Balsamo, G.; Bauer, P.; et al. The ERA-Interim reanalysis: Configuration and performance of the data assimilation system. *Q. J. R. Meteorol. Soc.* **2011**, *137*, 553–597. [CrossRef]
49. Rodell, M.; Houser, P.; Jambor, U.; Gottschalck, J.; Mitchell, K.; Meng, C.-J.; Arsenault, K.; Cosgrove, B.; Radakovich, J.; Bosilovich, M.; et al. The Global Land Data Assimilation System. *Bull. Am. Meteorol. Soc.* **2004**, *85*, 381–394. [CrossRef]
50. Miralles, D.G.; Holmes, T.R.H.; de Jeu, R.A.M.; Gash, J.H.; Meesters, A.G.C.A.; Dolman, A.J. Global land-surface evaporation estimated from satellite-based observations. *Hydrol. Earth Syst. Sci.* **2011**, *15*, 453–469. [CrossRef]
51. Gelaro, R.; McCarty, W.; Suárez, M.J.; Todling, R.; Molod, A.; Takacs, L.; Randles, C.A.; Darmenov, A.; Bosilovich, M.G.; Reichle, R.; et al. The Modern-Era Retrospective Analysis for Research and Applications, Version 2 (MERRA-2). *J. Clim.* **2017**, *30*, 5419–5454. [CrossRef]
52. Merlin, O.; Escorihuela, M.J.; Mayoral, M.A.; Hagolle, O.; Al Bitar, A.; Kerr, Y. Self-calibrated evaporation-based disaggregation of SMOS soil moisture: An evaluation study at 3 km and 100 m resolution in Catalunya, Spain. *Remote Sens. Environ.* **2013**, *130*, 25–38. [CrossRef]
53. Merlin, O.; Rüdiger, C.; Al Bitar, A.; Richaume, P.; Walker, J.P.; Kerr, Y.H. Disaggregation of SMOS Soil Moisture in Southeastern Australia. *IEEE Trans. Geosci. Remote Sens.* **2012**, *50*, 1556–1571. [CrossRef]
54. Zhao, T.; Shi, J.; Lv, L.; Xu, H.; Chen, D.; Cui, Q.; Jackson, T.J.; Yan, G.; Jia, L.; Chen, L.; et al. Soil moisture experiment in the Luan River supporting new satellite mission opportunities. *Remote Sens. Environ.* **2020**, *240*, 111680. [CrossRef]
55. Gao, Q.; Makhoul, E.; Escorihuela, M.J.; Zribi, M.; Seguí, P.Q.; García, P.; Roca, M. Analysis of Retrackers' Performances and Water Level Retrieval over the Ebro River Basin Using Sentinel-3. *Remote Sens.* **2019**, *11*, 718. [CrossRef]